RSC Advances

PAPER

View Article Online
View Journal | View Issue

Cite this: *RSC Adv.*, 2021, **11**, 21153

Stephapierrines A–H, new tetrahydroprotoberberine and aporphine alkaloids from the tubers of *Stephania pierrei* Diels and their anti-cholinesterase activities†

Waraluck Chaichompoo,[a] Pornchai Rojsitthisak, *[ab] Wachirachai Pabuprapap,[c] Yuttana Siriwattanasathien,[c] Pathumwadee Yotmanee,[c] Woraphot Haritakun[d] and Apichart Suksamrarn[c]

Received 27th April 2021
Accepted 18th May 2021

DOI: 10.1039/d1ra03276c

rsc.li/rsc-advances

Eight new alkaloids, which are four new tetrahydroprotoberberine alkaloids, stephapierrines A–D (**1–4**), and four new aporphine alkaloids, stephapierrines E–H (**5–8**), together with three new naturally occurring alkaloids (**9–11**) and thirty-four known alkaloids (**12–45**) were isolated from the tubers of *Stephania pierrei* Diels. The structures of the new compounds were elucidated by spectroscopic analysis and physical properties. The structures of the known compounds were characterized by comparison of their spectroscopic data with those previously reported. Compound **42** exhibited the strongest acetylcholinesterase (AChE) inhibitory activity, which was more active than galanthamine, the reference drug. Compound **23** showed the highest butyrylcholinesterase (BuChE) inhibitory activity, which was also more active than galanthamine. Molecular docking studies are in good agreement with the experimental results.

Introduction

Alzheimer's disease (AD) is the major progressive chronic neurodegenerative disease, accounting for an estimated 60–80% of cases of patients suffering from dementia worldwide.[1] It is deterioration in cognitive function affecting memory, thinking, learning, judgement, and behavior which is ultimately interfering with the ability of the person to perform daily tasks.[2] In 2019, over 50 million people were living with dementia worldwide. This number is expected to increase to 152 million by 2050.[3] The impact of AD is not only substantial in economic terms for health care resources and medical services, but also represents the extensive human costs to countries, societies, families, and individuals. Previously reported hypotheses on the progression of AD pathologies included cholinergic dysfunction, amyloid plaques, neurofibrillary tangles, neuroinflammation, and mitochondrial dysfunction, as well as oxidative stress, which are the major hallmarks of AD.[4] Cholinergic hypothesis is one of the theories for AD pathology. Acetylcholine (ACh) neurotransmitter used by cholinergic neurons is considered to play a critical role in the peripheral and central nervous systems.[5] Acetylcholinesterase (AChE) and butyrylcholinesterase (BuChE) are the biologically important enzymes that hydrolyze ACh.[6] In addition, BuChE was associated with AD pathology, such as amyloid-beta (Aβ) plaques.[7] It has been reported that acetylcholinesterase inhibitors (AChEIs) decrease the level of AChE in the brains of AD patients, which resists cerebral neurotransmitter acetylcholine metabolism and prolongs ACh action at the synapses.[8] Thus, the inhibitions of AChE and BuChE to protect and enhance the ACh levels in patients have been the most attractive therapeutic strategy. US Food and Drug Administration (FDA)-approved medications are palliative and offer only temporary modulate the symptoms by changing the level of neurotransmitters in the brain. Donepezil, rivastigmine, and galanthamine are currently the only three AChEIs available in clinics while memantine is an *N*-methyl-D-aspartate receptor (NMDAR) antagonist.[9] However, these AChEI drugs cannot stop or reverse disease progression and cause several side effects.[10] Due to these issues, there is a crucial need to find an effective and safe disease-modifying medication to overcome AD and the research for new medications with potential clinical value seems to be necessary.

[a]*Department of Food and Pharmaceutical Chemistry, Faculty of Pharmaceutical Sciences, Chulalongkorn University, Bangkok 10330, Thailand. E-mail: pornchai.r@chula.ac.th; Fax: +66-2-254-5195; Tel: +66-2-218-8310*

[b]*Natural Products for Aging and Chronic Diseases Research Unit, Chulalongkorn University, Bangkok 10330, Thailand*

[c]*Department of Chemistry and Center of Excellence for Innovation in Chemistry, Faculty of Science, Ramkhamhaeng University, Bangkok 10240, Thailand*

[d]*Program in Chemical Technology, Faculty of Science and Technology, Suan Dusit University, Bangkok 10700, Thailand*

† Electronic supplementary information (ESI) available. See DOI: 10.1039/d1ra03276c

Plant-derived natural products have long been and will continue to be extremely important as the most promising source of biologically active compounds. A great potential is expected for indigenous plants to be used as a source of new drugs. Among these natural products, alkaloids are considered to be the most promising candidates for the treatment of AD due to their complex nitrogen-containing structures.[11] Many alkaloids that are active cholinesterase inhibitors have already been described in various families, for example, the Menispermaceae family.[12]

The genus *Stephania* belongs to the Menispermaceae family, a large family of approximately 65 genera and 350 species, distributed in temperate regions of the world. The plants of the genus *Stephania* are slender climbers with peltate and membranous leaves. The plants of this genus are commonly used in Asian folk medicine to treat a wide range of biological activities including malaria, fever, dysentery, and tuberculosis.[13] At least 15 species in the genus *Stephania* have been found distributed throughout Thailand.[14] *Stephania pierrei* Diels, known in Thai as Sabu-lueat, is a medicinal plant regularly used in traditional remedies and as herbal medicine to treat body oedema, migraine, and heart disease, which are primarily distributed in Cambodia, Thailand, and Vietnam.[15] The reported data showed that several types of alkaloids had been isolated from this plant species, including aporphine, tetrahydroprotoberberine, tetrahydrobenzylisoquinoline, and miscellaneous compounds.[16,17] However, the anti-cholinesterase activity of this plant has not been reported. From our preliminary investigation on phytochemicals with cholinesterase inhibitory activities from Thai medicinal plants, we found that the active crude extracts of the tubers of *S. pierrei* showed inhibitory activities on AChE and BuChE. Accordingly, we report herein the isolation, structure elucidation, and absolute configuration assignments of eight new alkaloids (**1–8**), and three new naturally occurring alkaloids (**9–11**), together with thirty-four known alkaloids (**12–45**) from the tuber extracts of *S. pierrei*. Most of the isolated compounds were also evaluated for their AChE and BuChE inhibitory activities. For further insight into the experimental results, *in silico* studies were performed.

Results and discussion

The tubers of *S. pierrei* were extracted successively with *n*-hexane, EtOAc, and MeOH. Preliminary screening of the hexane, EtOAc and MeOH extracts of this plant revealed significant *in vitro* cholinesterase inhibitory activities towards AChE with IC_{50} ranges from 1.01–20.95 ng mL^{-1} and exhibited BuChE inhibitory activity with the IC_{50} values of 2.76–17.46 ng mL^{-1}. These active extracts were therefore subjected to chromatographic isolation for the active principles. Based on the spectroscopic analysis and the physical properties, the chemical structures of the isolated compounds were elucidated and characterized as eight previously undescribed alkaloids, which are four new tetrahydroprotoberberine alkaloids stephapierrines A–D (**1–4**) and four new aporphine alkaloids stephapierrines E–H (**5–8**). Three new naturally occurring alkaloids, *O*,*N*-diacetylasimilobine (**9**),[18] *N*-acetamidesecocrebanine (**10**)[19] and 2,3-didemethyltetrahydropalmatine (**11**),[20] together with thirty-four known alkaloids (**12–45**) were identified. The previously described alkaloids were identified as stepholidine (**12**),[21] discretamine (**13**),[22] tetrahydropalmatine (**14**),[23] *N*-methylstepholidine (**15**),[21] cyclanoline (**16**),[21] *N*-methyltetrahydropalmatine (**17**),[23] jatrorrhizine (**18**),[24] palmatine (**19**),[25] dehydrocorydaline (**20**),[26] pseudodehydrocorydaline (**21**),[27] roemerine (**22**),[28] (−)-stephanine (**23**),[29] (−)-isolaureline (**24**),[30] crebanine (**25**),[23] dicentrine (**26**),[31] (−)-ushinsunine (**27**),[32] (−)-ayuthianine (**28**),[29] sukhodianine (**29**),[33] (−)-*N*-fonnylanonaine (**30**),[32] (−)-*N*-methylasimilobine (**31**),[32] (−)-asimilobine (**32**),[32] (−)-asimilobine-2-*O*-β-D-glucoside (**33**),[16,34] lanuginosine (**34**),[35] dicentrinone (**35**),[36] oxocrebanine (**36**),[35] 8-methoxyuvoriopsine (**37**),[37] dehydroroemerine (**38**),[38] dehydrostephanine (**39**),[39] dehydroisolaureline (**40**),[40] dehydrocrebanine (**41**),[40] dehydrodicentrine (**42**),[41] (−)-crebanine-β-*N*-oxide (**43**),[42] coclaurine (**44**)[43] and salutaridine (**45**)[44] by physical and spectroscopic data comparisons with those of the literature values (see Fig. 1). The spectroscopic (IR, ^1H and ^{13}C NMR and mass) spectra of the new compounds **1–8**, and the ^1H and ^{13}C NMR spectra, together with the specific optical rotations and mass spectral data of compounds **9–45** are presented in the ESI.†

Stephapierrine A (**1**) was assigned the molecular formula $C_{21}H_{23}NO_5$ as deduced from the HR-ESI-TOF-MS at *m*/*z* 370.1633 $[M + H]^+$ and NMR data. This alkaloid and all other isolated alkaloids gave positive orange coloration with Dragendorff's reagent. The IR spectrum indicated the presence of a hydroxy group (3380 cm^{-1}), an acetoxy group (1761 cm^{-1}) and aromatic rings (1608 and 1514 cm^{-1}). The ^1H NMR data (Table 1) showed two singlet methoxy signals at δ_H 3.79 and 3.85 (each 3H, s), and an acetoxy methyl proton signal at δ_H 2.30 (s), together with two *ortho*-coupled aromatic protons at δ_H 6.90 and 6.88 (each 1H, d, J = 8.8 Hz, H-11 and H-12) and two aromatic singlet protons at δ_H 6.78 and 6.58 (1H each, s, H-1 and H-4). The ^{13}C NMR (Table 2) and DEPT spectra showed twenty-one carbon signals which included twelve aromatic carbons between δ_C 110.6 and 147.7, one carbonyl carbon (δ_C 169.1), three methyl carbons (δ_C 20.8, 55.9 and 60.6), four methylene carbons (δ_C 28.7, 36.0, 51.3 and 53.5), and one methine carbon (δ_C 58.8). The seventeen-carbon and one-nitrogen skeleton of **1** suggested a tetraoxygenated tetrahydroprotoberberine alkaloid core structure.[45,46] This was further confirmed by the presence of two adjacent methylenes as multiplet signals at δ_H 2.68 and 3.18 (H-5) and δ_H 2.68 and 3.21 (H-6), methylene signals at δ_H 3.59 and 4.22 (each d, J = 15.7 Hz, H-8), methylene signals at δ_H 2.90 (dd, J = 16.4, 12.2 Hz) and 3.28 (dd, J = 16.4, 3.2 Hz) (H-13), together with a partially overlapping signal at δ_H 3.64 (H-13a). The COSY correlations of these protons are shown in Fig. 2. The structure of **1** was similar to that of stepholidine (**12**).[21] The main difference between the ^1H NMR spectrum of **12** and that of **1** was the presence of an acetoxy methyl signal at δ_H 2.30 (1H, s) which was proven to be at C-10 by HMBC correlations between CO*CH*$_3$ (δ_H 2.30) and *CO*CH$_3$ (δ_C 169.1), and C-10 (δ_C 141.0) (see Fig. 2). The HMBC correlations between the OH signal (δ_H 5.52) and C-1 (δ_C 111.2) and C-2 (δ_C 144.0) allowed the location of this phenolic function at C-2. The location of the methoxy groups at C-3 and C-9 were assigned according to the correlations of the methoxy signals at δ_H 3.85 and 3.79 with the carbons at δ_C 145.2 (C-3) and δ_C 147.7 (C-9), respectively. The structure of

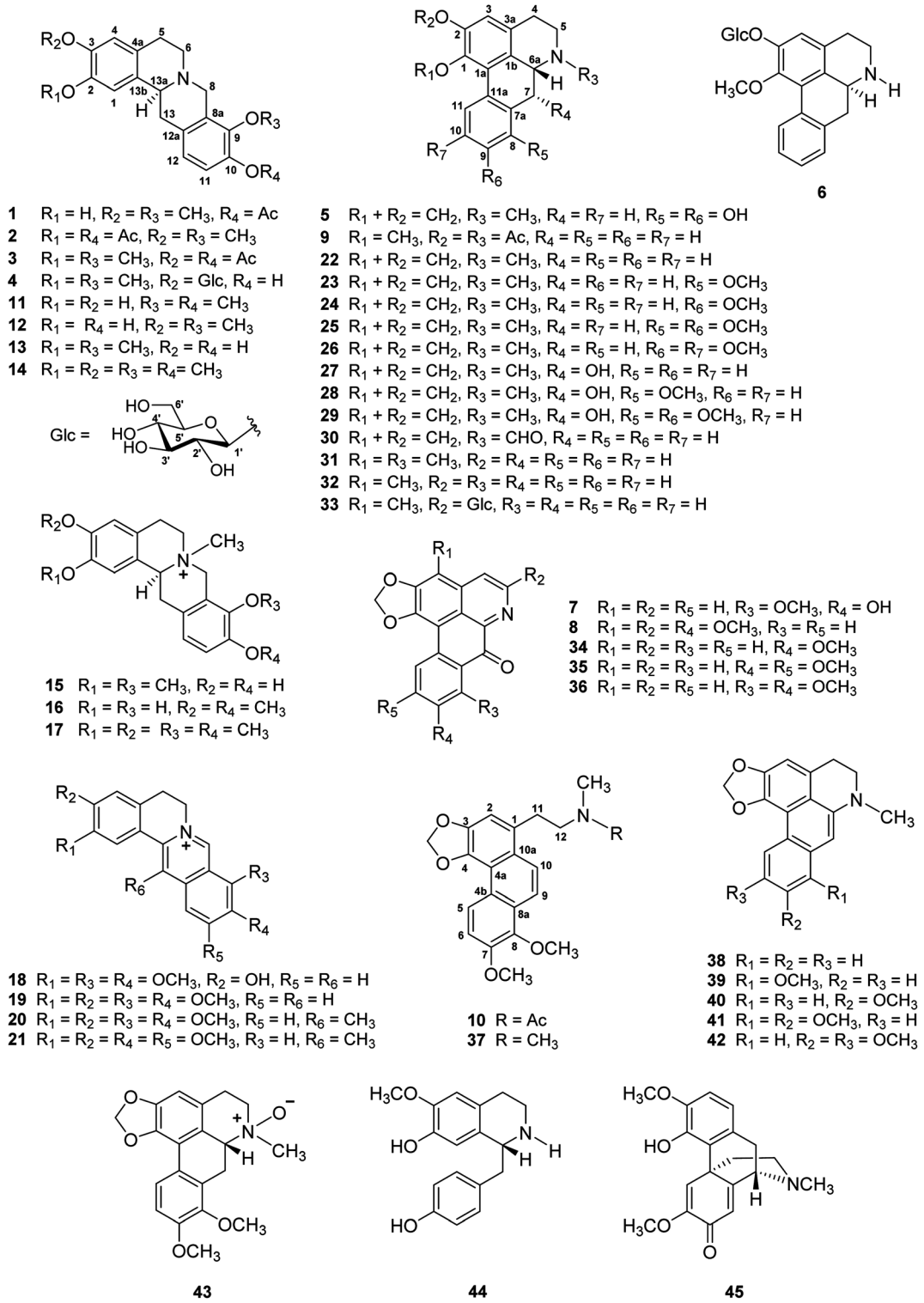

Fig. 1 Structures of the isolated compounds **1**–**45** from the tubers of *Stephania pierrei*.

compound **1** was confirmed by key HMBC correlations from H-1 to C-3, C-4a and C-13a, H-4 to C-2 and C-5, H-8 to C-6, C-9, C-12a and C-13a, and H-13 to C-13b (see Fig. 2). The structure of compound **1** was further confirmed by the following key NOESY correlations: CH_3O-3/H4, H-6/H-5 and H-8, CH_3O-9/H-8, and H-13a/H-1 and H-13 (Fig. 3). The absolute configuration of C-13a of this class of alkaloids has been established, for example, by stereoselective asymmetric synthesis.[47] The negative sign of specific optical rotation of **1** is consistent with an α-orientation of hydrogen at C-13a. The absolute configuration of **1** was confirmed by the electronic circular dichroism (ECD) spectrum (Fig. S234†), which was similar to those reported for

Table 1 ^{1}H NMR data (400 MHz) of compounds **1–4** and **11**[a]

Position	**1**[b]	**2**[b]	**3**[b]	**4**[c]	**11**[d]
1	6.78 s	6.89 s	6.89 s	6.92 s	6.68 s
4	6.58 s	6.68 s	6.79 s	6.93 s	6.63 s
5	2.68 m	2.71 m	2.64[f]	2.69[f]	2.54[f]
	3.18 m	3.14[e]	3.08[f]	3.07 m	2.89 m
6	2.68 m	2.63 m	2.62[f]	2.64[f]	2.42[f]
	3.21 m	3.15[e]	3.15[f]	3.20 m	3.08[f]
8	3.59 d (15.7)	3.51 d (15.7)	3.54 d (15.9)	3.35 d (15.6)	3.35[e]
	4.22 d (15.7)	4.17 d (15.7)	4.18 d (15.9)	4.19 d (15.6)	4.02 d (15.7)
11	6.90 d (8.8)	6.86 d (8.4)	6.88 d (9.2)	6.72 d (8.2)	6.67 d (8.2)
12	6.88 d (8.8)	6.86 d (8.4)	6.88 d (9.2)	6.80 d (8.2)	6.71 d (8.2)
13	2.90 dd (16.4, 12.2)	2.85 dd (16.1, 11.2)	2.90 dd (16.1, 11.3)	2.73 dd (16.1, 11.0)	2.50 dd (15.7, 12.3)
	3.28 dd (16.4, 3.2)	3.23 dd (16.1, 3.4)	3.27 dd (16.1, 3.5)	3.41 dd (16.1, 3.5)	3.14 dd (15.7, 3.4)
13a	3.64[f]	3.55 dd (11.2, 3.4)	3.60 dd (11.3, 3.5)	3.58 dd (11.0, 3.5)	3.34[e]
2-OCH$_3$			3.82 s	3.86 s	
3-OCH$_3$	3.85 s	3.80 s			
9-OCH$_3$	3.79 s	3.79 s	3.79 s	3.80 s	3.71 s
10-OCH$_3$					3.73 s
2-OCOCH$_3$		2.29 s			
3-OCOCH$_3$			2.29 s		
10-OCOCH$_3$	2.30 s	2.30 s	2.31 s		
1-OH					8.68 s
2-OH	5.52 s				9.06 s
1′				4.88 d (7.5)	
2′				3.45 dd (8.7, 7.5)	
3′				3.48 t (8.7)	
4′				3.38[e]	
5′				3.38[e]	
6′				3.68 dd (12.1, 5.2)	
				3.85 dd (12.1, 1.7)	

[a] Assignments were based on ^{1}H–^{1}H COSY, HMQC, HMBC, and NOESY experiments; chemical shifts (δ) are given in ppm. [b] Recorded in $CDCl_3$. [c] Recorded in CD_3OD. [d] Recorded in DMSO-d_6. [e] Overlapping signal. [f] Partially overlapping signal.

tetrahydroprotoberberine alkaloids,[48,49] with negative Cotton effects at 204 nm ($\Delta\varepsilon$ −10.69), 243 nm ($\Delta\varepsilon$ −50.55) and 287 nm ($\Delta\varepsilon$ −6.61). Thus, the absolute configuration of C-13a was established as *S*-configuration (Fig. 1). Accordingly, compound **1** was identified as 10-*O*-acetylstepholidine.

The molecular formula of stephapierrine B (**2**) was determined to be $C_{23}H_{25}NO_6$ on the basis of HR-ESI-TOF-MS (*m*/*z* 412.1747 $[M + H]^+$) and NMR data. The IR spectrum showed absorption bands of acetoxy groups (1753 cm^{-1}) and aromatic rings (1623 and 1511 cm^{-1}). The ^{1}H and ^{13}C NMR data (Tables 1 and 2) showed similar spectral features to those of compound **1**. The significant difference was the presence of an additional acetoxy group at δ_H 2.29, and δ_C 20.8 and 169.3. The HMBC experiments showed correlations between AcO-2 (δ_H 2.29) and C-2 (δ_C 138.0), whereas H-1 (δ_H 6.89) correlated with C-2, C-3 (δ_C 149.2), C-4a (δ_C 130.0), C-13a (δ_C 58.6) and C-13b (δ_C 133.1) (see Fig. 2). It should be noted that the presence of the acetoxy group at the 2-position resulted in 0.11 and 8.5 ppm down-field shifts of H-1 and C-1 resonances, respectively, as compared with those of compound **1**. These observations indicated that the acetoxy group should be located at the 2-position. Compound **2** showed the negative sign of specific optical rotation as that of compound **1**, suggesting the same *S*-configuration or α-orientation of hydrogen at C-13a. This was confirmed by the similar ECD curve of **2** (Fig. S234†) that exhibited similar negative Cotton effects at 206 nm ($\Delta\varepsilon$ −14.21), 240 nm ($\Delta\varepsilon$ −63.97) and 286 nm ($\Delta\varepsilon$ −2.69), respectively. Compound **2** was therefore identified as 2,10-di-*O*-acetylstepholidine (see Fig. 1).

Stephapierrine C (**3**) was deduced to have the molecular formula $C_{23}H_{25}NO_6$ by combined analysis of the HR-ESI-TOF-MS *m*/*z* 412.1748 $[M + H]^+$ and NMR data. The IR spectrum displayed the absorption bands of acetoxy groups (1758 cm^{-1}) and aromatic rings (1619 and 1512 cm^{-1}). The ^{1}H and ^{13}C NMR data of **3** (Tables 1 and 2) were similar to those of compound **1**. The main differences were the presence of an additional acetoxy group (δ_H 2.29, and δ_C 20.8 and 169.2) and the methoxy group should be placed at C-2 as was supported by the HMBC correlation between the CH_3O-2 and C-2 (δ_C 149.3) (see Fig. 2). This was confirmed by the NOESY correlation between the CH_3O-2 and H-1 (δ_H 6.89) (see Fig. 3). The location of the acetoxy group at C-3 was also supported by the HMBC correlation of the acetoxy methyl proton (δ_H 2.29) with C-3 (δ_C 138.1), together with the correlations of H-4 with C-2, C-3, C-4a (δ_C 127.1), C-5 (δ_C 28.6), and C-13b (δ_C 133.6). Compound **3** exhibited the same negative specific rotation and displayed a similar ECD spectrum as those of compound **1** (Fig. S234†), suggesting the same *S*-configuration at C-13a. Therefore, compound **3** was established as 3,10-di-*O*-acetyldiscretamine (see Fig. 1).

Table 2 ^{13}C NMR data (100 MHz) of compounds **1–4** and **11**[a]

Position	**1**[b]	**2**[b]	**2**[b]	**4**[c]	**11**[d]
1	111.2	119.7	121.2	111.5	114.8
2	144.0	138.0	149.3	150.0	147.3
3	145.2	149.2	138.1	147.1	144.6
4	110.6	112.3	122.6	118.6	111.7
4a	125.5	130.0	127.1	129.2	124.7
5	28.7	29.4	28.6	29.7	28.5
6	51.3	51.2	51.1	53.1	51.1
8	53.5	53.7	53.8	55.3	53.5
8a	128.4	129.2	129.3	128.5	125.7
9	147.7	147.7	147.7	145.5	143.2
10	141.0	141.0	141.0	149.3	146.0
11	121.4	121.2	124.2	116.8	112.3
12	124.3	124.2	124.2	125.9	123.7
12a	133.4	133.7	135.9	127.6	128.3
13	36.0	36.4	36.4	37.0	35.8
13a	58.8	58.6	59.1	61.4	58.6
13b	130.3	133.1	133.6	133.4	129.9
2-OCH$_3$			56.0	57.5	
3-OCH$_3$	55.9	55.8			
9-OCH$_3$	60.6	60.6	60.6	60.9	59.2
10-OCH$_3$					55.5
2-OCO$\underline{\text{CH}}_3$		20.8			
2-O$\underline{\text{CO}}$CH$_3$		169.3			
3-OCO$\underline{\text{CH}}_3$			20.8		
3-O$\underline{\text{CO}}$CH$_3$			169.2		
10-OCO$\underline{\text{CH}}_3$	20.8	20.6	20.6		
10-O$\underline{\text{CO}}$CH$_3$	169.1	169.2	169.2		
1′				103.3	
2′				75.4	
3′				78.3	
4′				71.9	
5′				78.7	
6′				63.0	

[a] Assignments were based on ^{1}H–^{1}H COSY, HMQC, HMBC, and NOESY experiments; chemical shifts (δ) are given in ppm. [b] Recorded in $CDCl_3$. [c] Recorded in CD_3OD. [d] Recorded in DMSO-d_6.

The molecular formula of stephapierrine D (**4**) was determined to be $C_{25}H_{31}NO_9$ from the HR-ESI-TOF-MS (*m*/*z* 490.2056 $[M + H]^+$) and NMR data. Its IR data indicated the presence of hydroxy groups (3314 cm^{-1}) and aromatic rings (1611 and 1512 cm^{-1}). The ^{1}H and ^{13}C NMR data of **4** (Tables 1 and 2) were similar to those of discretamine (**13**), which has also been isolated from *S. pierrei* in the present work. The significant differences were the presence of an anomeric proton signal at δ_H 4.88 (1H, d, J = 7.5 Hz, H-1′) along with signals of sugar residue at δ_H 3.38 (2H, overlapping, H-4′ and H-5′), 3.45 (1H, dd, J = 8.7 and 7.5 Hz, H-2′), 3.48 (1H, t, J = 8.7, H-3′), 3.68 (1H, dd, J = 12.1 and 5.2 Hz, H_a-6′), and 3.85 (1H, dd, J = 12.1 and 1.7 Hz, H_b-6′) in the ^{1}H NMR spectrum, and from the carbon resonances at δ_C 103.3 (C-1′), 78.29 (C-3′ and C-5′), 75.4 (C-2′), 71.9 (C-4′), and 63.0 (C-6′) in the ^{13}C NMR spectrum. The large coupling constant of the anomeric proton signal together with the remaining characteristic ^{1}H and ^{13}C signals of the sugar residue suggested this sugar moiety to be a β-glucoside.[16,50]

The anomeric proton signal showed correlation with the anomeric carbon signal at δ_C 103.3 (C-1′) in the HMQC spectra (Figs. S66–S68†). The sequence of the glucose unit connected to C-3 of the aglycone was deduced from the HMBC correlations of the anomeric H-1′ (δ_H 4.88) with the aglycone carbon signals at C-3 (δ_C 147.1), C-3′ (δ_C 78.3) and C-5′ (δ_C 78.7), indicating the attachment of β-D-glucose at C-3 (see Fig. 2). In addition, the ^{1}H–^{1}H COSY correlations, H-1′/H-2′, H-2′/H-3′, H-3′/H-4′, H-4′/H-5′, and H-5′/H-6′, were observed (see Fig. 2). Moreover, the NOESY correlations of H-1′ and H-4 (δ_H 6.93), H-3′ (δ_H 3.48) and H-5′ (δ_H 3.38) (Fig. 3) were also key interactions to support this glucoside structure. The β-D-glucosyl nature of this sugar residue was confirmed by enzymatic hydrolysis of **4** with β-glucosidase[51] and the hydrolysis products were identified to be discretamine (**13**)[22] and D-glucose by TLC comparison with authentic **13** and D-glucose. Furthermore, the location of the methoxy group at C-2 was supported by the HMBC correlation between the CH_3O-2 signal and C-2 (δ_C 150.0) (see Fig. 2) and this was further confirmed by the NOESY correlation between the CH_3O-2 and H-1 (δ_H 6.92) (see Fig. 3). As the substituent on tetrahydroprotoberberine molecule, including a glucose moiety, does not exert a considerable effect on the optical rotation and ECD spectrum,[49,52] the same sign of optical rotation and similar ECD curve of compound **4** (Fig. S234†) when compared with those of compounds **1–3** has led to a conclusion that the absolute configuration at C-13a of **4** is *S*. On the basis of these findings, compound **4** is the glucoside analogue of discretamine (**13**).[22] Compound **4** was therefore identified as discretamine 3-*O*-β-D-glucopyranoside (see Fig. 1).

The molecular formula of stephapierrine E (**5**) was deduced to be $C_{18}H_{18}NO_4$ from HR-ESI-TOF-MS (*m*/*z* 312.1224 $[M + Na]^+$) and NMR data. The IR spectrum exhibited the absorption bands of the hydroxy group (3383 cm^{-1}) and aromatic rings (1603 and 1575 cm^{-1}). The ^{1}H NMR spectrum (Table 3) showed the characteristic signals of an aporphine alkaloid as a singlet *N*-methyl proton at δ_H 2.64 (3H, s, NCH_3), a singlet aromatic proton at δ_H 6.50 (1H, s, H-3), two *ortho*-coupled aromatic protons at δ_H 7.46 (1H, d, J = 8.4 Hz, H-11) and 6.71 (1H, d, J = 8.4 Hz, H-10), one methine proton at δ_H 3.20 (1H, dd, J = 14.1 and 4.5 Hz, H-6a), one coupled methylene protons at δ_H 3.09 and 2.64 (2H, overlapping signal, H-5), and another coupled methylene protons at δ_H 3.14 and 2.68 (2H, overlapping signal, H-4). Additional methylene protons at the 7-position appeared at δ_H 3.69 (1H, dd, J = 14.5 and 4.5 Hz) and δ_H 2.19 (1H, dd, J = 14.5 and 14.1 Hz). In addition, the spectrum displayed resonances due to a methylenedioxy proton at δ_H 6.02 and 5.88 (each 1H, d, J = 1.1 Hz). The ^{13}C NMR and DEPT-135 spectra (Table 4) revealed the presence of 18 signals which included one methylenedioxy carbon, three methylene carbons, four methine carbons, nine quaternary carbons, and one *N*-methyl carbon. The sixteen-carbon and one-nitrogen skeleton of **5** suggested an aporphine alkaloid core structure.[41,53,54] The spectroscopic data for **5** was similar to those of crebanine (**25**),[23] especially the substitution patterns on the molecule. The significant difference is the absence of two methoxy signals in the NMR spectra of **5** (Tables 3 and 4). The structure of compound **5** was further confirmed by HMBC and NOESY experiments (see Fig. 2 and 3). The absolute configuration of compound **5** was deduced by optical rotation experiments. The negative sign of specific

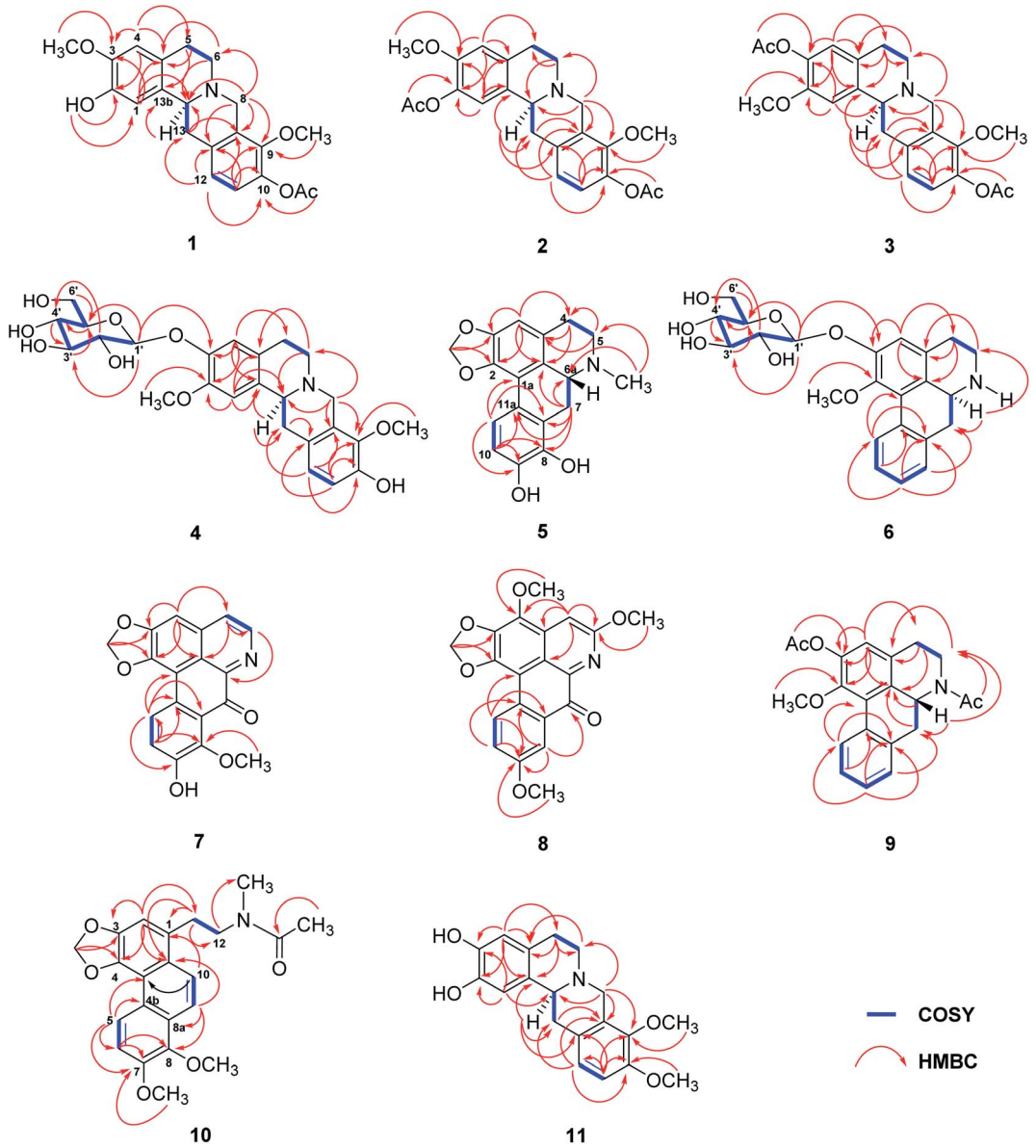

Fig. 2 $^{1}H-^{1}H$ COSY and HMBC correlations of compounds **1–11**.

optical rotation suggested that the absolute configuration of C-6a was *R*, or the hydrogen at the C-6a position is in the β-orientation.[29] This was supported by the ECD spectrum (Fig. S235†). The structure of **5** was therefore elucidated as di-*O*-demethylcrebanine.

The molecular formula of stephapierrine F (**6**) was established as $C_{23}H_{27}NO_7$ from the HR-ESI-TOF-MS (*m*/*z* 430.1856 $[M + H]^+$) and NMR data. The IR spectrum indicated the presence of hydroxy groups (3311 cm^{-1}) and aromatic rings (1593 cm^{-1}). The ^{1}H NMR data (Table 3) showed the presence of a methoxy signal at δ_H 3.72, four adjacent aromatic hydrogens δ_H 7.31 (1H, dd, $J = 7.1$, 1.2 Hz, H-8), 7.26 (1H, ddd, $J = 7.5$, 7.1, 1.2 Hz, H-9), 7.32 (1H, ddd, $J = 7.6$, 7.5, 1.2 Hz, H-10), and 8.33 (1H, brd, $J = 7.6$ Hz, H-11), which were ascribed to the hydrogens of the unsubstituted D ring of the aporphine alkaloid.[54] In addition, the ^{1}H NMR spectrum revealed the presence of a sugar unit with its anomeric proton appearing at δ_H 4.96 (1H, d, $J = 7.6$ Hz, H-1′). The remaining sugar proton signals H-2′ to H-6′ are in the region δ_H 3.38–3.92 exhibiting similar features to those of compound **4**. The ^{13}C NMR spectrum (Table 4) showed 23 carbon resonances, of which five methines and one methylene were assigned to the β-glucopyranose moiety, suggested that **6** was an aporphine glucoside. The existence of a β-D-glucosyl moiety was confirmed by enzymatic hydrolysis[51] in a similar manner to compound **4**. The sugar linkage was determined by the HMBC correlations of H-1′ with C-2 (δ_C 153.1), C-3′ (δ_C 78.8) and C-5′ (δ_C 78.8) (see Fig. 2).[50] The HMBC correlation between the methoxy proton at δ_H 3.72 and a carbon resonance at δ_C 147.9 (C-1) confirmed that the location of the methoxy group was placed to C-1. Additionally, the structural assignment for compound **6** was supported by the analysis of its NOESY spectrum (see Fig. 3); the H-1′ signal displayed a key interaction with

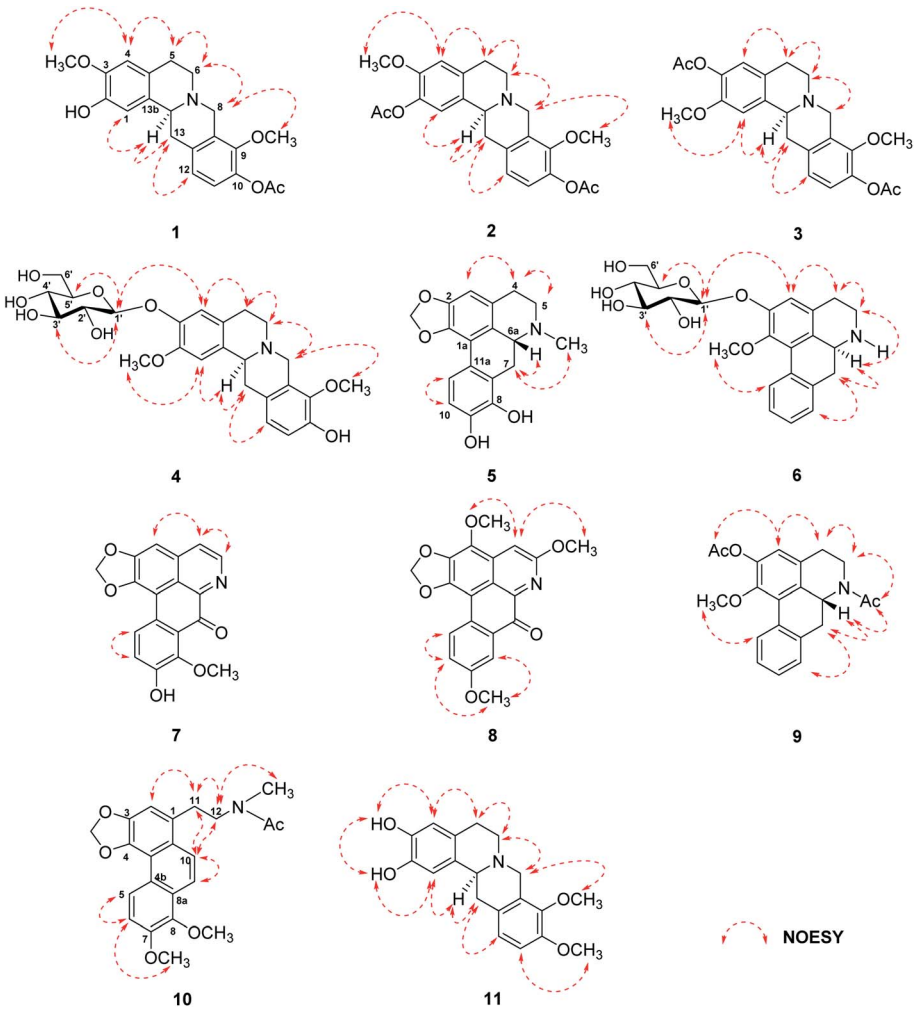

Fig. 3 NOESY correlations of compounds **1–11**.

H-3, H-3′ and H-5′. Moreover, H-6a (δ_H 4.11) displayed key interactions with H-7 (δ_H 2.87 and 3.03) and H-8 (δ_H 7.31), whereas CH_3O-1 (δ_H 3.72) showed correlation to H-11 (δ_H 8.33). The ^1H and ^{13}C NMR spectra were consistent with those of (−)-asimilobine-2-*O*-β-D-glucoside (**33**).[16] However, the sign of specific optical rotation of **6** was opposite to that of **33**. The reported specific optical rotation of **33** was −107 (c = 0.1, MeOH).[16] It is therefore possible that these two alkaloids are C-6a enantiomers. The ECD of **6** has therefore been determined and it was found that its ECD curve exhibited opposite Cotton effects to those of compounds **5** (see Fig. S235†). This led to a conclusion that the absolute configuration at C-6a of **6** was *S*. It is normal for the aporphine alkaloids to exist at different chirality at the asymmetric carbon C-6a.[57] Based on these data, the structure of compound **6** was established as (+)-asimilobine 2-*O*-β-D-glucopyranoside.

Stephapierrine G (**7**) was assigned the molecular formula $C_{18}H_{11}NO_5$ as determined from the HR-ESI-TOF-MS at m/z 344.0523 $[M + Na]^+$ and NMR data. The IR spectrum showed absorption bands of hydroxy groups (3276 cm^{-1}) and a conjugated carbonyl group (1638 cm^{-1}). The ^{13}C NMR spectrum in combination with the DEPT-135 experiment (Table 4) indicated the presence of 18 carbon atoms belonging to eleven quaternary carbons, five methine carbons, one methylene carbon, and one methyl carbon. The ^1H NMR spectrum (Table 3) revealed characteristic resonances for protons and carbons at C-4 and C-5 of an aporphine unit as a pair of doublet signals at δ_H 7.76 and 8.56 (each 1H, d, J = 5.2 Hz), which connected to δ_C 125.8 and 144.9, respectively. Two singlet signals at δ_H 7.07 (1H, s) and 6.28 (2H, s) attaching to carbons at δ_C 102.7, and 104.4, respectively, were assigned to proton signals at C-3 and methylenedioxy protons, respectively. Two doublets at δ_H 7.15 and 8.19 (each 1H, d, J = 8.8 Hz) were attributed to two *ortho*-coupled aromatic protons at C-10 and C-11, respectively. In addition, a singlet signal at δ_H 3.92 (3H, s) was assigned to the methoxy proton at C-8. This assignment was confirmed by the HMBC correlations of the CH_3O-8 and H-10 with C-8 (δ_C 152.0). The correlations of H-11 with C-1a (δ_C 110.4), C-7a (δ_C 126.3), C-9 (δ_C 157.9), and C-11a (δ_C 124.9) suggested the location of the hydroxy group at C-9 (see Fig. 2). The carbonyl carbon resonance at δ_C 184.1 together with a high-field resonance of its adjacent carbon (δ_C 126.3, C-7a) supported that **7** was a 7-oxoaporphine

Table 3 ^{1}H NMR data (400 MHz) of compounds **5–9**[a]

Position	**5**[b]	**6**[b]	**7**[b]	**8**[c]	**9**[b]
3	6.50 s	7.08 s	7.07 s		6.91 s
4	2.68[d]	2.94 dd (14.9, 2.5)	7.76 d (5.2)	7.82 s	2.73[e]
	3.14[d]	3.22[e]			2.86[e]
5	2.64[d]	3.20[e]	8.56 d (5.2)		3.27[e]
	3.09[d]	3.59 brdd (12.6, 5.3)			4.12 brdd (13.2, 2.0)
6a	3.20 dd (14.1, 4.5)	4.11 dd (13.9, 4.3)			4.97 dd (13.8, 3.8)
7	2.19 dd (14.5, 14.1)	2.87 dd (13.9, 13.8)			2.79 t (13.8)
	3.69 dd (14.5, 4.5)	3.03 dd (13.8, 4.3)			2.96 dd (13.8, 3.8)
8		7.31 dd (7.1, 1.2)		8.03 s	7.25–7.32[e]
9		7.26 ddd (7.5, 7.1, 1.2)			7.25–7.32[e]
10	6.71 d (8.4)	7.32 ddd (7.6, 7.5, 1.2)	7.15 d (8.8)	7.30 d (9.0)	7.25–7.32[e]
11	7.46 d (8.4)	8.33 brd (7.6)	8.19 d (8.8)	8.66 d (9.0)	8.30 brd (7.7)
OCH_2O	5.88 d (1.1)				
6.02 d (1.1)		6.28 s	6.40 s		
1-OCH_3		3.72 s			3.53 s
3-OCH_3				4.03 s	
5-OCH_3				3.82 s	
8-OCH_3			3.92 s		
9-OCH_3				4.03 s	
2-$OCOCH_3$					2.32 s
N–CH_3	2.64 s				
N–$COCH_3$					2.21 s
1′		4.96 d (7.6)			
2′		3.54 dd (8.9, 7.6)			
3′		3.48 t (8.9)			
4′		3.38 dd (8.9, 8.6)			
5′		3.48 brdd (8.6, 6.0)			
6′		3.69 dd (12.0, 6.0)			
		3.92 dd (12.0, 2.1)			

[a] Assignments were based on ^{1}H–^{1}H COSY, HMQC, HMBC, and NOESY experiments; chemical shifts (δ) are given in ppm. [b] Recorded in $CDCl_3$. [c] Recorded in CD_3OD. [d] Overlapping signal. [e] Partially overlapping signal.

scaffold.[58,59] Furthermore, the NOESY correlations of H-3 with H-4 and H-4 with H-5 (Fig. 3) as well as additional key HMBC correlations (Fig. 2) confirmed the structure of compound **7** to be a 7-oxoaporphine analogue. The spectroscopic data suggested that **7** is closely related to oxocrebanine (**36**),[35] which has also been isolated from *S. pierrei* in the present work. Comparison of the NMR data of compounds **7** and **36** revealed that **7** is 9-de-*O*-methyloxocrebanine. Thus, compound **7** was concluded to be 1,2-methylenedioxy-8-methoxy-9-hydroxyoxoaporphine.

The sodiated molecular ion of the HR-ESI-TOF-MS of stephapierrine H (**8**) at *m*/*z* 388.0772 and the NMR data have led to the assignment of the molecular formula $C_{20}H_{15}NO_6$. The IR spectrum indicated the presence of a conjugated carbonyl group (1651 cm^{-1}). The ^{1}H and ^{13}C NMR data (Tables 3 and 4) showed two *ortho*-coupled aromatic protons at δ_H 7.30 and 8.66 (each 1H, d, J = 9.0 Hz, H-10 and H-11),[58] together with two singlet protons at δ_H 7.82 and 8.03 (each 1H, s, H-4, and H-8). The remaining signals were assignable to three methoxys at δ_H 3.82 (3H, s, CH_3O-5) and 4.03 (6H, s, CH_3O-3, and CH_3O-9), together with a methylenedioxy signal at δ_H 6.40 (2H, s). The foregoing ^{1}H NMR data, together with the ^{13}C NMR data (Table 4) suggested **8** to be an oxoaporphine type alkaloid.[46,58,59] The HMBC experiments (see Fig. 2) confirmed the structure of compound **8**. The structure of **8** was also confirmed by the NOESY correlations (see Fig. 3). On the basis of these data, the structure of compound **9** was established as 1,2-methylenedioxy-3,5,9-trimethoxyoxoaporphine.

Compound **9** was assigned the molecular formula $C_{21}H_{21}NO_4$ as determined from the HR-ESI-TOF-MS (*m*/*z* 374.1363 $[M + Na]^+$). The IR spectrum exhibited absorption bands of the acetoxy group (1761 cm^{-1}) and amide group (1636 cm^{-1}). The ^{1}H and ^{13}C NMR spectra (Tables 3 and 4) suggested an aporphine alkaloid core structure.[41,53,54] The COSY correlations of these protons are shown in Fig. 2. The ^{1}H NMR data showed the typical resonance of the *N*-acetyl signal at δ_H 2.21. The aromatic protons showed four adjacent signals for H-8, H-9 and H-10 in the range δ_H 7.25–7.32 and at δ_H 8.30 (1H, brd, J = 7.7 Hz) for H-11, which were attributed to the hydrogens of the unsubstituted D ring of the aporphine alkaloid.[54] These observations were confirmed by ^{1}H–^{1}H COSY and HMBC experiments (see Fig. 2). The significant down-field shift of H-11 is the characteristic of this class of alkaloids.[55,56] Furthermore, an aromatic singlet signal at δ_H 6.91 (H-3), a methoxy signal at δ_H 3.53 and an acetoxy proton signal at δ_H 2.32 were observed. The ^{1}H and ^{13}C NMR spectra of **9** were in agreement with the structure of *O*,*N*-diacetylasimilobine (**9**),[18] which has been synthesized from asimilobine (**32**).[32] This was confirmed by the

Table 4 ^{13}C NMR data (100 MHz) of compounds **5–9**[a]

Position	**5**[b]	**6**[b]	**7**[b]	**8**[c]	**9**[b]
1	144.0	147.9	154.3	150.6	150.0
1a	119.0	127.1	110.4	115.3	129.8
1b	126.5	129.0	123.3	119.9	133.8
2	148.9	153.1	148.3	147.7	145.4
3	107.6	117.6	102.7	143.7	123.8
3a	127.5	128.5	137.9	132.6	131.9
4	29.7	27.7	125.8	107.9	31.4
5	55.0	43.4	144.9	156.6	43.5
6a	63.9	54.9	147.1	132.6	52.7
7	27.5	36.1	184.1	174.7	35.0
7a	123.3	135.7	126.3	126.9	138.4
8	143.5	129.6	152.0	108.1	129.9
9	146.6	129.6	157.9	150.8	129.7
10	114.5	129.1	126.3	113.4	129.5
11	120.7	129.9	125.9	123.0	128.7
11a	124.6	133.2	124.9	120.3	132.7
OCH_2O	102.4		104.4	102.8	
1-OCH_3		61.7			61.3
3-OCH_3				61.3	
5-OCH_3				56.2	
8-OCH_3			61.7		
9-OCH_3				56.2	
2-OCO$\underline{CH}_3$					22.7
2-O$\underline{CO}CH_3$					171.4
N–CH_3	44.0				
$N-CO\underline{CH}_3$					21.1
$N-\underline{CO}CH_3$					172.5
1′		103.0			
2′		75.4			
3′		78.8			
4′		71.9			
5′		78.8			
6′		63.1			

[a] Assignments were based on ^{1}H–^{1}H COSY, HMQC, HMBC, and NOESY experiments; chemical shifts (δ) are given in ppm. [b] Recorded in $CDCl_3$. [c] Recorded in CD_3OD.

Table 5 ^{1}H and ^{13}C NMR data (400 MHz for ^{1}H, and 100 MHz for ^{13}C) of compound **10**[a]

	10[b]	
Position	δ_H	δ_C
1		129.8
2	7.06 s	110.1
3		145.0
4		141.9
4a		117.1
4b		127.3
5	8.80 d (9.2)	123.7
6	7.28 d (9.2)	112.7
7		149.9
8		143.2
8a		123.6
9	7.92 d (9.6)	118.6
10	7.81 d (9.6)	122.9
10a		125.1
11	3.29 m	31.4
12	3.14 m	61.9
OCH_2O	6.19 s	100.9
7-OCH_3	4.00 s	56.3
8-OCH_3	3.98 s	61.2
N–CH_3	2.81 s	46.9
$N-CO\underline{CH}_3$	2.09 s	19.5
$N-\underline{CO}CH_3$		169.7

[a] Assignments were based on ^{1}H–^{1}H COSY, HMQC, HMBC, and NOESY experiments; chemical shifts (δ) are given in ppm. [b] Recorded in $CDCl_3$.

HMBC experiments (Fig. 2) and the NOESY experiment (Fig. 3). It is noteworthy that the H-11 down-field shift in **9** (δ_H 8.30) was more pronounced than that of compound **5** (δ_H 7.46), and this was due to the vicinity of the methylenedioxy group in **5**.[55,56] The negative sign of specific optical rotation of **9** suggested that the absolute configuration of C-6a was *R*, or the hydrogen at the C-6a position is in the β-orientation.[29] This was supported by the ECD spectrum (Fig. S235†). Based on these data, the structure of compound **9** was identical to (−)-*O*,*N*-diacetylasimilobine.[18] Compound **9** has been reported in the present work as a naturally occurring alkaloid for the first time.

The molecular formula of compound **10** was deduced to be $C_{22}H_{23}NO_5$ from the HR-ESI-TOF-MS at *m*/*z* 382.1258 $[M + H]^+$. The IR spectrum indicated the presence of an acetoxy group (1751 cm^{-1}). The ^{1}H and ^{13}C NMR features of **10** (Table 5) were similar to those of 8-methoxyuvoriopsine (**37**),[37] the significant difference of which was the presence of an *N*-acetyl group, and the absence of an *N*-methyl signal. The rest of the ^{1}H and ^{13}C NMR data were consistent with the core structure of both compounds. The structure of **10** was confirmed by HMBC and NOESY analyses (see Fig. 2 and 3, respectively). Compound **10** has been reported as a structurally modified analogue from crebanine (**25**) and was called *N*-acetamidesecocrebanine,[19] though some of the reported NMR spectroscopic data do not match with our data. This compound has thus been reported in the present work as a naturally occurring alkaloid for the first time.

Compound **11** was assigned the molecular formula $C_{19}H_{21}NO_4$ as deduced from the HR-ESI-TOF-MS at *m*/*z* 328.1542 $[M + H]^+$ and NMR data. The IR spectrum revealed the presence of hydroxy groups (3380 cm^{-1}). The ^{1}H and ^{13}C NMR data (Tables 1 and 2) showed similar patterns to those of tetrahydropalmatine (**14**),[23] except that the ^{1}H NMR spectrum of **11** at the aromatic region was less well-defined. The NMR spectra of compound **11** showed only two methoxy signals at δ_H 3.71 (δ_C 59.2) and δ_H 3.73 (δ_C 55.5). Placement of the two methoxy groups at C-9 and C-10 was based on HMBC correlations of the CH_3O-9 proton signal with C-9 (δ_C 143.2), CH_3O-10 signal with C-10 (δ_C 146.0), H-8 and H-11 with C-9, and H-12 with C-10. This was further confirmed by NOESY correlations between CH_3O-9 and H-8, and correlation between CH_3O-10 and H-11. In addition, the locations of the hydroxy groups at C-2 and C-3 were deduced from HMBC correlations of H-1 with C-2 (δ_C 147.3) and C-3 (δ_C 144.6), and H-4 with C-2 and C-3 (Fig. 2). The positions of the hydroxy groups were confirmed by NOESY correlations (see Fig. 3). Compound **11** was therefore the 2,3-di-*O*-demethylated analogue of tetrahydropalmatine (**14**).[23] Compound **11** was previously detected as one of the demethylated metabolites of compound **14** from rat's urine by ultra high-performance liquid

chromatography–tandem mass spectrometric analysis.[20] Thus, we report herein the spectroscopic data of **11**, 2,3-didemethyltetrahydropalmatine, which was identified as a new naturally occurring alkaloid in the plant species.

Cholinesterase inhibitory activities

Several reports on the cholinesterase inhibitory activities of alkaloids from the *Stephania* plant species by different groups of researchers have appeared.[21,60–63] In the present work, most of the isolated compounds were evaluated for their acetylcholinesterase (AChE) and butyrylcholinesterase (BuChE) inhibitory activities and the results are shown in Table 6. The well-known AChE and BuChE inhibitor, galanthamine, was used as the reference drug. Compound **42** exhibited the highest inhibitory activity against AChE (IC_{50} 1.09 μM) followed by compound **38** (IC_{50} 1.21 μM), with the IC_{50} values of 1.21 and 1.09 μM, respectively, which were slightly more active than and comparable to galanthamine (IC_{50} 1.21 μM). Compounds **22**, **26**, **28**, **29**, **39** and **45** showed high inhibitory activities with the IC_{50} values of 2.85–8.32 μM, followed by compounds **1**, **2**, **13**, **15**, **17**, **18**, **21**, **23–25**, **27**, **37**, **41** and **44** which exhibited moderate AChE inhibitory activity with the IC_{50} values of 11.33–41.47 μM. Moreover, compounds **3**, **14**, **19**, **30**, **32**, **34**, **35** and **40** showed weak activity with the IC_{50} values of 71.28–265.82 μM, whereas compounds **11**, **12**, **33**, **36** and **43** were inactive to the test.

Table 6 Anti-cholinesterase activities of alkaloids from the tubers of *Stephania pierrei*[a]

	AChE[b]	BuChE[c]
Compounds	IC_{50} (μM)	IC_{50} (μM)
1	41.47 ± 0.77	Inactive[d]
2	15.41 ± 0.54	Inactive[d]
3	149.63 ± 1.33	63.12 ± 0.83
11	Inactive[d]	Inactive[d]
12	Inactive[d]	221.16 ± 1.62
13	26.99 ± 0.58	109.33 ± 0.97
14	71.28 ± 1.90	65.35 ± 0.80
15	11.33 ± 0.15	13.52 ± 0.59
17	21.16 ± 0.40	234.34 ± 1.08
18	12.25 ± 0.44	31.46 ± 0.20
19	152.59 ± 0.81	Inactive[d]
21	18.31 ± 1.55	32.82 ± 0.34
22	8.32 ± 0.12	2.85 ± 0.08
23	11.34 ± 0.20	2.80 ± 0.07
24	11.94 ± 0.39	16.58 ± 0.54
25	17.37 ± 0.22	10.51 ± 0.27
26	6.11 ± 0.38	26.41 ± 0.43
27	17.63 ± 0.67	7.42 ± 0.16
28	6.12 ± 0.63	5.87 ± 0.06
29	4.30 ± 0.28	22.47 ± 0.10
30	140.15 ± 0.83	Inactive[d]
32	141.47 ± 0.82	10.08 ± 0.15
33	Inactive[d]	175.55 ± 1.45
34	73.08 ± 0.33	13.60 ± 0.30
35	265.82 ± 0.80	Inactive[d]
36	Inactive[d]	Inactive[d]
38	1.21 ± 0.09	3.34 ± 0.02
39	2.85 ± 0.24	3.26 ± 0.05
40	147.18 ± 0.71	20.32 ± 0.39
41	32.49 ± 0.52	14.11 ± 0.25
42	1.09 ± 0.02	5.57 ± 0.15
43	Inactive[d]	150.57 ± 0.54
44	40.86 ± 0.67	20.46 ± 0.42
45	7.49 ± 0.66	7.83 ± 0.11
Galanthamine[e]	1.21 ± 0.11	3.59 ± 0.07

[a] Data represent as IC_{50} values in μM ± S.D. of three independent experiments. [b] Acetylcholinesterase. [c] Butyrylcholinesterase. [d] Inactive at 0.1 mg mL^{-1}. [e] Galanthamine was used as the reference drug.

For the BuChE inhibitory activities, compounds **23** and **22** displayed high inhibitory activity, with the IC_{50} values of 2.80 and 2.85 μM, respectively, which were approximately 1.3-fold more active than galanthamine (IC_{50} 3.59 μM), followed by compounds **39** and **38**, which also showed high activity of 3.26 and 3.34 μM, respectively, which were slightly more active than galanthamine. Compounds **27**, **28**, **42** and **45** showed high inhibitory activity with the IC_{50} values in the range 5.57–7.83 μM. Furthermore, compounds **15**, **18**, **21**, **24–26**, **29**, **32**, **34**, **40**, **41** and **44** exhibited moderate inhibitory activity with the IC_{50} values of 10.08–22.47 μM, followed by compounds **3**, **12–14**, **17**, **33** and **43** that showed weak anti-BuChE activity with the IC_{50} values of 63.12–234.34 μM. Compounds **1**, **2**, **11**, **19**, **30**, **35** and **36** were inactive to the test.

Structure–activity relationship (SAR) studies

Structure–activity relationship (SAR) studies indicated that, for anti-AChE activity, the aporphine alkaloids are the most active group. The protoberberine alkaloids are only moderately active, weakly active, or inactive. SAR discussion mainly focused on the aporphine alkaloids. Among the aporphines bearing the 2,3-methylenedioxy and 6-*N*-methyl functions, there are three groups of them, based on the structural nature around the C-6a and C-7 positions. For the saturated analogues, the aporphine group, the parent compound **22** exhibited moderate AChE inhibitory activity, with the IC_{50} of 8.32 μM (see Table S1†). Introduction of a methoxy function on the 8- and 9-positions to give the mono-methoxy analogues **23** and **24** resulted in a decrease in activity (IC_{50} of 11.34 and 11.94 μM). Introduction of the second methoxy group of **24** to the dimethoxy analogue **25** further reduced AChE inhibitory activity (IC_{50} 17.37 μM). However, introduction of a methoxy group to the 10-position of **24** to the analogue **26** caused a considerable increase in activity (IC_{50} 6.11 μM). The presence of the 10-methoxy function seemed to enhance anti-AChE activity. It should be mentioned that the presence of the 6-*N*-formyl, instead of the *N*-methyl, group as well as the absence of the 6-methyl group, resulted in a sharp decrease in activity, as in the case of compounds **30** and **32** that exhibited very weak anti-AChE activity (IC_{50} 140.15 and 141.47 μM). It should also be noted that introduction of oxygen to the amino function of **25** to give the *N*-oxide analogue **43** resulted in complete loss of AChE inhibitory activity. In the presence of an α-hydroxy group at the 7-position, an increase in inhibitory activity was observed for compounds **28** and **29** (IC_{50} 6.12 and 4.30 μM), except for compound **27** that a decrease in activity was observed. Unfortunately, only three 7-hydroxy analogues of this group were isolated. The most highly active analogues are those

Table 7 Summary of the binding interactions and energies of AChE and BuChE complexed with alkaloids from the tubers of *Stephania pierrei*

Compound	Residue	Interaction	Distance (Å)	$\Delta G_{docking}$ (Kcal mol^{-1})	IC_{50} (μM)
AChE-inhibitor interaction					
38	F295	Hydrogen bond	2.82	−9.57	1.21
	W286	Pi–Pi	4.02, 4.92, 5.36		
	S293	Pi–Pi	3.63		
	F297	Pi–Pi	5.16		
	Y341	Pi–Pi	4.93		
42	R296	Hydrogen bond	1.70	−8.95	1.09
	W286	Pi–Pi	4.15, 3.71, 5.46, 4.13, 5.59, 5.56		
	Y124	Pi–Pi	5.78		
	S293	Pi–Pi	4.30		
Galanthamine	G121	Pi–σ	3.76	−7.91	1.21
	F338	Pi–Pi	5.94		
BuChE-inhibitor interaction					
22	W82	Pi–Pi	4.68, 5.40, 5.32, 5.35	−8.07	2.85
		Pi–σ	3.89		
	T120	Pi–Pi	3.36		
23	W82	Pi–Pi	4.95, 5.72, 4.38, 5.26	−8.28	2.80
			3.86, 5.26		
		Pi–σ	3.42, 3.87		
38	W82	Pi–Pi	4.64, 5.52, 5.21, 5.42	−8.01	3.34
	T120	Pi–σ	3.37		
39	W82	Pi–Pi	5.88, 4.56, 5.31, 5.20	−7.89	3.26
			5.04		
Galanthamine	W82	Pi–σ	3.83	−7.41	3.59

with a 6a,7-unsaturated analogues, the dehydroaporphines. Compounds **38**, **39** and **42** were strongly active (IC_{50} 1.21, 2.85 and 1.09 μM, respectively). Compounds **38** and **42** were respectively as active as and more active than galanthamine, the reference drug. However, the analogues **40** and **41** showed weak activity (IC_{50} 147.18 and 32.49 μM), suggesting that, while the more rigid dehydroaporphine skeleton contributed to high anti-AChE property, the number and position of the oxygenation patterns highly affected the activity of this group of alkaloids.

For the anti-BuChE activity, the aporphine alkaloids are also the most active group. Almost all protoberberine alkaloids are weakly active or inactive. SAR discussion was mainly on the aporphine alkaloids as well as that of the anti-AChE activity. In the aporphine group, compound **23** exhibited high BuChE inhibitory activity,

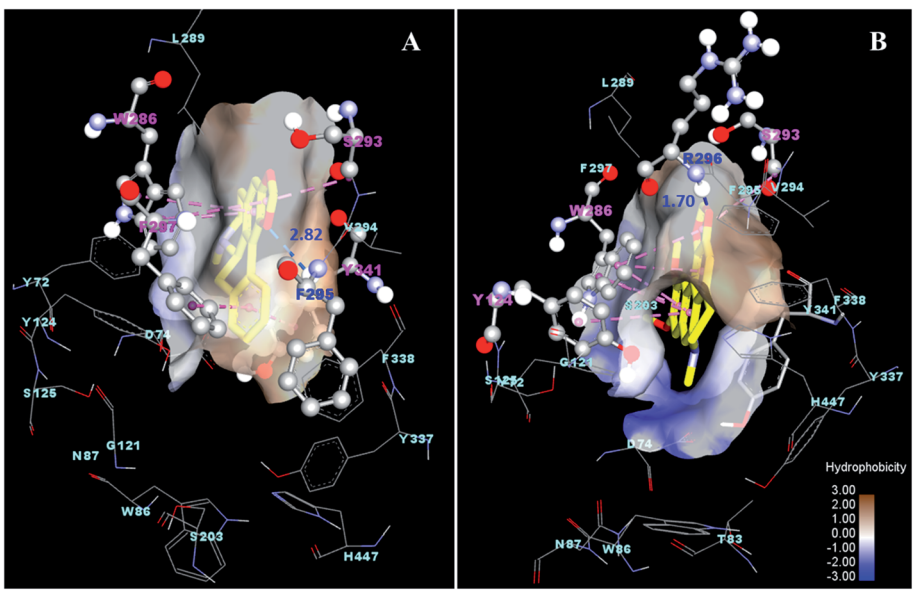

Fig. 4 Binding interaction of docking poses of the ligands (yellow) in the vicinity of the target protein AChE (gray). (A) Binding mode of compound **38** and (B) binding mode of compound **42**. The residues of the interaction site are shown as ball and stick. The blue and pink dashed lines represent hydrogen bonding and hydrophobic interaction, respectively.

followed by **22** (IC_{50} of 2.80 and 2.85 μM, respectively (see Table S1†)). The methoxy group on the 8-position seemed to enhance the activity. In contrast, the 9-methoxy group caused a 5.8-fold decrease in the activity of compound **24** (IC_{50} 16.58 μM) when compared with compound **22**. While the anti-AChE activity of the 8,9-dimethoxy analogue **25** was 2.8-fold less active than the 9,10-dimethoxy analogue **26**, the anti-BuChE activity of **25** was 2.5-fold higher than that of **26** (Table 6). This implied that the oxygen functions at the 8-, 9- and 10-positions differently contributed to cholinesterase inhibitory activities of the aporphine alkaloids. It should also be noted that the presence of the 6-*N*-formyl group in the analogue **30** caused inactivity in this compound and the absence of the 6-*N*-methyl group in the analogue **32** did not cause a sharp decrease of anti-BuChE property as that occurred in the anti-AChE case since it exhibited anti-BuChE activity with IC_{50} of 10.08 μM. It should also be mentioned that, in going from the amino function in **25** to the corresponding *N*-oxide function in **43**, a sharp decrease in BuChE inhibitory activity was observed. In the presence of an α-hydroxy group at the 7-position of the aporphine core structure, in contrast to most of the aporphine group, an approximately 2-fold decrease in inhibitory activity was observed for compounds **27**, **28** and **29** (IC_{50} 7.42, 5.87 and 22.47 μM, respectively). For the third group of the aporphine analogues, the dehydroaporphines, a slight decrease in activity was observed for compounds **38**, **39**, **40** and **41** (IC_{50} 3.34, 3.26, 20.32 and 14.11 μM, respectively). However, the analogue **42** showed a 4.7-fold increase in anti-BuChE activity (IC_{50} 5.57 μM). This implied that the more rigid dehydroaporphine skeleton and the number and position of the methoxy groups contributed to the anti-BuChE activity of this group of alkaloids.

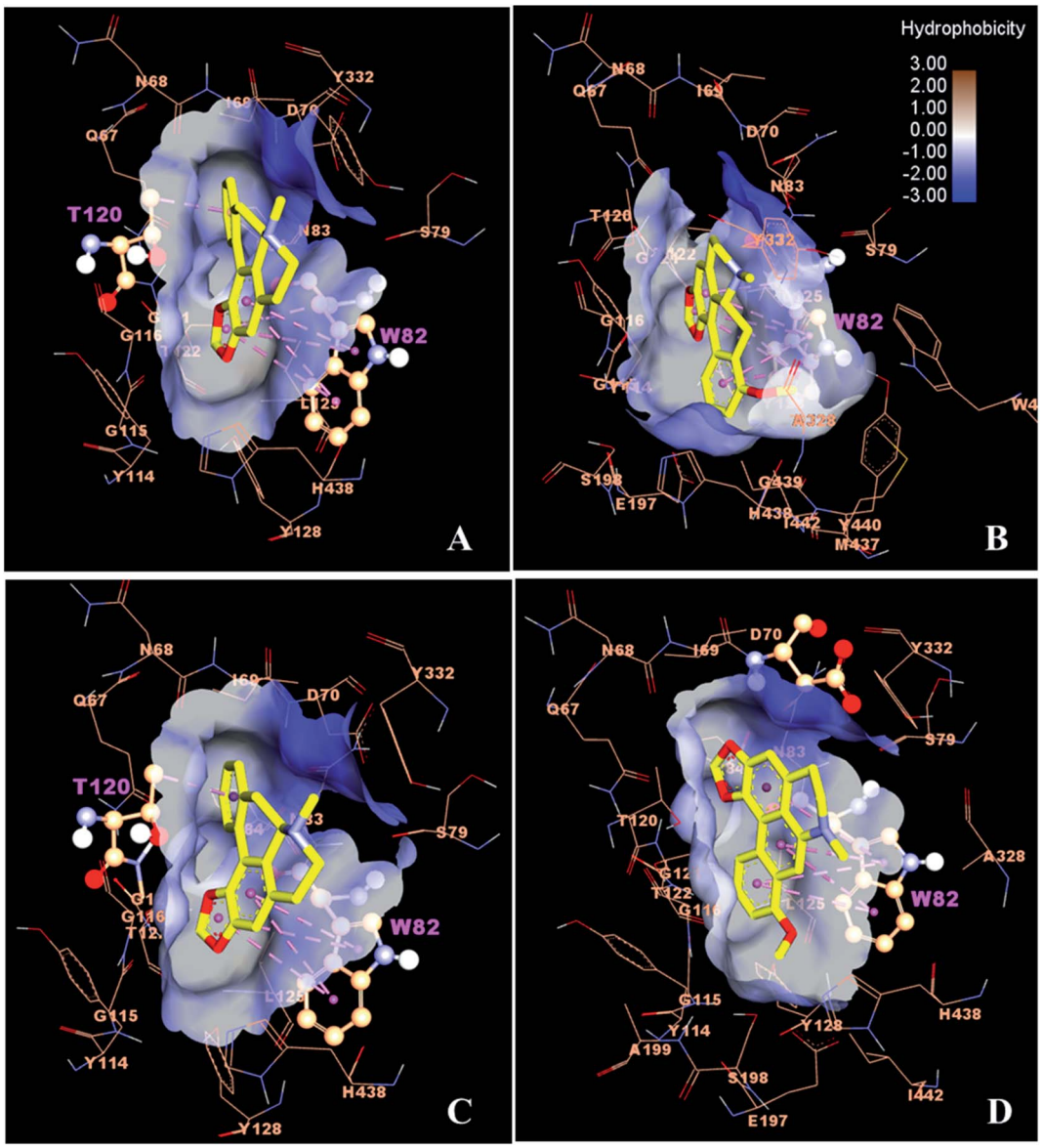

Fig. 5 Binding interaction of ligands (yellow) with BuChE enzyme (orange); (A–D) Binding pose of active compounds **22**, **23**, **38** and **39**. The dashed pink bond shows the hydrophobic interaction with the site residue (ball and stick).

Molecular docking study of the interaction between the potent alkaloids and cholinesterase enzymes

Molecular docking was performed using the AutoDock program to gain insight into the possible interaction of the potent inhibitory activity of the alkaloids with the enzymes AChE (compounds **38** and **42**) and BuChE (compounds **22**, **23**, **38** and **39**). The binding energy (ΔG, kcal mol^{-1}) and interaction residues of the alkaloids within the enzyme binding site obtained from the best ranked and the most populated conformation of the docking calculation are summarized in Table 7.

The active site of AChE and BuChE consists of five regions such as the catalytic triad (CT), the anionic site (AS), the acyl pocket (AC), the oxyanion hole (OAH) and the peripheral anionic site (PAS). Thus, the amino acids of S203, E334, H447, W86, Y133, F337, F338, of F295, F297, G121, G122, A204, Y72, D74, Y124, W286 and Y341 are considered as active residues of AChE,[64] while W82, Y128, F330, F331, L286, V288, G116, G117, A199, D70 and Y332 are identified as the key residues of BuChE binding gorge.[65]

As can be seen from Fig. 4, the docking result shows that compounds **38** and **42** were well occupied in the active site of AChE, where compound **38** could form a hydrogen bond with residue F295 and hydrophobic interactions with W286, S293, F297 and Y341. In contrast, compound **42** formed a hydrogen bond with R296 and strong Pi–Pi interactions with W286, Y124 and S293. The binding free energies of compounds **38** and **42** were similarly found to be −9.57 and −8.95 kcal mol^{-1}, respectively, which possessed higher binding affinity with the AChE binding site compared to galanthamine (ΔG of −7.91 kcal mol^{-1}).

The best conformations of the docked complexes of BuChE and compounds **22**, **23**, **38** and **39** are shown in Fig. 5. The results showed that these alkaloids mainly interacted with BuChE by forming Pi–Pi interactions with the key residue W82. The free energy of binding for all complexes is similar, being about −8 kcal mol^{-1}. Interestingly, the binding free energies of these alkaloids show good binding affinity with the BuChE binding site compared to galanthamine (−7.41 kcal mol^{-1}).

The molecular docking results showed that, for the alkaloids isolated from the tubers of *S. pierrei*, compounds **38** and **42** as well as compounds **22**, **23**, **38** and **39** exhibited good binding affinity towards AChE and BuChE, respectively, which is in agreement with the experimental IC_{50} values.

Experimental

General experimental procedures

Optical rotations were measured on a JASCO-1020 polarimeter. Electronic Circular Dichroism (ECD) was recorded on a JASCO J-810 spectropolarimeter. UV spectra were collected on a Shimadzu UV 1800 spectrophotometer. IR spectra were recorded in the ATR mode using a PerkinElmer FT-IR Spectrum 400 spectrophotometer. ^{1}H and ^{13}C NMR spectra were recorded on a Bruker ASCEND 400 FT-NMR spectrometer, operating at 400 MHz (^{1}H) and 100 (^{13}C) MHz. HR-ESI-TOF-MS spectra were measured with a Bruker micrOTOF-QII mass spectrometer. Unless otherwise indicated, column chromatography was carried out using Merck silica gel 60 (particle sizes less than 0.063 mm) and GE Healthcare Sephadex LH-20. For thin-layer chromatography (TLC), Merck pre-coated silica gel 60 F_{254} plates were used. Spots on TLC were detected under UV light and by spraying with anisaldehyde-H_2SO_4 reagent followed by heating.

Plant material

The tubers of *Stephania pierrei* were collected from Prachin Buri Province, Thailand in 2019 and the plant species was identified by Assoc. Prof. Nopporn Dumrongsiri, Ramkhamhaeng University. A voucher specimen is deposited at the Faculty of Science, Ramkhamhaeng University, Thailand (Apichart Suksamrarn, No. 101).

Extraction and isolation

The fresh tubers of *S. pierrei* (1.5 kg) were sliced, air-dried, milled, and macerated successively with *n*-hexane, EtOAc, and MeOH at room temperature. The filtered solution of each extraction was evaporated under reduced pressure at 40–45 °C to give the hexane (2.8 g), ethyl acetate (3.3 g), and methanol (4.5 g) extracts, respectively.

The crude hexane extract (2.5 g) was fractionated by column chromatography, using a gradient solvent system of *n*-hexane, *n*-hexane–EtOAc, EtOAc, EtOAc–MeOH and MeOH with increasing amounts of the more polar solvent. The eluates were examined by TLC and 7 combined fractions (H1–H7) were obtained. Fraction H1 (280.0 mg) was column chromatographed eluting with a gradient system of *n*-hexane–CH_2Cl_2 (10 : 0.1 to 10 : 4) to give 5 subfractions (H1.1–H1.5). Subfraction H1.2 (23.0 mg) was rechromatographed over silica gel eluting with *n*-hexane–CH_2Cl_2 (10 : 0.5) to yield compound **38** (5.0 mg). Subfraction H1.3 (200 mg) was subjected to column chromatography eluting with *n*-hexane–CH_2Cl_2 (10 : 1) to afford compounds **39** (15.0 mg), **40** (1.6 mg), **41** (20.0 mg), and **42** (2.4 mg). Subfraction H1.4 (15.0 mg) was rechromatographed over silica gel and eluting with *n*-hexane–EtOAc (10 : 0.3) to give compound **30** (1.3 mg). Subfraction H1.5 (18.0 mg) was subjected to column chromatography eluting with *n*-hexane–CH_2Cl_2–EtOAc (9 : 9 : 0.2) to afford compound **8** (2.2 mg). Fraction H2 (850 mg) was subjected to silica column chromatography eluting with the isocratic condition of CH_2Cl_2–MeOH (10 : 0.1) to give 5 subfractions (H2.1–H2.5). Subfraction H2.1 (290 mg) was rechromatographed over silica gel eluting with *n*-hexane–EtOAc (6 : 4) to yield compounds **25** (240 mg), and **3** (9.0 mg). Subfraction H2.2, H2.3, and H2.4 were identified to be compounds **22** (7.6 mg), **24** (15.3 mg), and **23** (433.0 mg). Fraction H3 (550.0 mg) was subjected to silica column chromatography eluting with a gradient condition of CH_2Cl_2–MeOH (10 : 0.1 to 10 : 0.3) to give 2 subfractions (H3.1–H3.2). Subfraction H3.1 (350.0 mg) was chromatographed eluting with CH_2Cl_2–MeOH (10 : 0.1) to afford compound **2** (50.6 mg) and compound **36** (150.0 mg). Subfraction H3.2 (150.0 mg) was rechromatographed over silica gel eluting with CH_2Cl_2–MeOH (10 : 0.2) to yield compound **26** (68.0 mg). Fraction H4 (180.0 mg) was subjected to silica column chromatography eluting

with the isocratic condition of CH_2Cl_2–MeOH (10 : 0.2) to give 4 subfractions (H4.1–H4.4). Subfraction H4.1 (75.0 mg) was chromatographed on Sephadex LH-20 column eluted with MeOH–CH_2Cl_2 (7 : 3) to yield compound **14** (15.0 mg). Subfraction H4.2 was identified to be compound **35** (5.5 mg). Subfraction H4.3 (15.0 mg) was chromatographed eluting with CH_2Cl_2–MeOH (10 : 0.3) to give compound **1** (2.5 mg). Subfraction H4.4 was identified to be compound **34** (2.0 mg). Fraction H5 (120.0 mg) was subjected to column chromatography eluting with the isocratic condition of CH_2Cl_2–MeOH (10 : 0.4) to give 3 subfractions (H5.1–H5.3). Subfraction H5.1 (25.0 mg) was chromatographed over silica gel eluting with CH_2Cl_2–MeOH (10 : 0.2), followed by column chromatography on Sephadex LH-20 eluted with MeOH to yield compound **7** (1.0 mg). Subfraction H5.3 (48.0 mg) was purified on a Sephadex LH-20 column eluted with MeOH to afford compound **17** (15.5 mg). Fraction H6 (80.0 mg) was chromatographed over silica gel and eluted under the isocratic condition of CH_2Cl_2–MeOH (10 : 0.8) to yield compounds **21** (12.0 mg), and **20** (2.5 mg). Subfraction H7 (125 mg) was chromatographed on Sephadex LH-20 column eluting with MeOH, followed by silica column chromatography, eluting with gradient solvent system of CH_2Cl_2–MeOH (10 : 1) to afford compound **19** (84.0 mg).

The crude EtOAc extract (3.0 g) was fractionated by column chromatography, using a gradient solvent system of EtOAc, EtOAc–MeOH and MeOH with increasing amounts of the more polar solvent. The eluates were examined by TLC and 3 combined fractions (E1–E3) were obtained. Fraction E1 (300.0 mg) was subjected to column chromatography eluting with an isocratic condition of CH_2Cl_2–MeOH (10 : 0.2) to give compounds **9** (1.5 mg), **31** (1.0 mg), **10** (1.2 mg), and **32** (3.2 mg). Fraction E2 (450.0 mg) was chromatographed on silica column eluting under isocratic condition of CH_2Cl_2–MeOH (10 : 0.5) to provide compounds **11** (3.4 mg), **13** (2.0 mg), and **12** (10.0 mg). Fraction E3 (150.0 mg) was subjected to silica column chromatography eluting under the isocratic condition of CH_2Cl_2–MeOH (10 : 1) to give compound **18** (5.0 mg).

The MeOH extract (4.2 g) was fractionated by column chromatography, using a gradient solvent system of EtOAc, EtOAc–MeOH, MeOH, and 5% water in MeOH with an increasing amount of the more polar solvent. The eluates were examined by TLC and 6 combined fractions (M1–M6) were obtained. Fraction M1 (450.0 mg) was subjected to column chromatography eluting under the isocratic condition of CH_2Cl_2–MeOH (10 : 1) to give 3 subfractions (M1.1–M1.3). Subfraction M1.2 (150.0 mg) was rechromatographed eluting with *n*-hexane–CH_2Cl_2–MeOH (40 : 50: 2) to afford compound **27** (30.0 mg). Subfraction M1.3 was identified to be compound **44** (29.1 mg). Fraction M2 (200.0 mg) was chromatographed over silica gel eluting with a gradient solvent system of CH_2Cl_2–MeOH (10 : 0.4) to give 4 subfractions (M2.1–M2.4). Subfraction M2.3 was identified to be compound **37** (3.9 mg).

Subfraction M2.4 (120.0 mg) was chromatographed eluting with the isocratic condition of CH_2Cl_2–MeOH (10 : 0.5) to yield compound **43** (20.6 mg). Fraction M3 (750.0 mg) was chromatographed on a silica gel column eluting under the isocratic condition of CH_2Cl_2–MeOH (10 : 0.5) to give 4 subfractions (M3.1–M3.4). Subfraction M3.2 was identified to be compound **45** (7.4 mg). Subfraction M3.3 (80.0 mg) was subjected to column chromatography eluting with CH_2Cl_2–MeOH (10 : 1) to afford compound **33** (9.0 mg). Subfraction M3.4 (30.0 mg) was rechromatographed over silica gel and eluted under the isocratic condition of CH_2Cl_2–MeOH (100 : 12) to yield compounds **16** (2.2 mg), and **15** (8.6 mg). Fraction M4 (150.0 mg) was purified by using a Sephadex LH-20 column eluting with MeOH, followed by silica column chromatography eluting with *n*-hexane–CH_2Cl_2–MeOH (40 : 50 : 10) to provide compound **4** (1.5 mg). Fraction M5 (280.0 mg) was chromatographed over silica gel eluting with an isocratic solvent system of CH_2Cl_2–EtOAc–MeOH (40 : 60 : 10) to give 4 subfractions (M5.1–M5.4). Subfraction M5.1 and M5.2 were identified as compounds **29** (8.8 mg) and **5** (1.3 mg), respectively. Subfraction M5.3 (80.0 mg) was rechromatographed over silica gel and eluted with CH_2Cl_2–EtOAc–MeOH (20 : 80 : 15) to give compound **28** (11.7 mg). Fraction M6 (80.0 mg) was chromatographed on Sephadex LH-20 column eluting with MeOH, followed by silica column chromatography, eluting with an isocratic solvent system of CH_2Cl_2–EtOAc–MeOH (20 : 60 : 20) to afford compound **6** (2.2 mg).

Compound 1. Yellowish amorphous powder; $[\alpha]_D^{25}$ −144.2 (*c* 0.29, MeOH); IR (ATR) ν_{max}: 3380, 2933, 1761, 1608, 1514, 1462, 1371, 1265, 1200, 1060, 875, 750 cm^{-1}; UV (MeOH) λ_{max} (log ε): 203 (4.62), 283 (3.51) nm; ECD (MeOH) λ_{max} ($\Delta\varepsilon$) 204 (−10.69), 243 (−50.55), 287 (−6.61) nm; ^{1}H-NMR ($CDCl_3$, 400 MHz), and ^{13}C-NMR ($CDCl_3$, 100 MHz) data: see Tables 1 and 2; ESI-TOF-MS *m*/*z* 370.1633 $[M + H]^+$ (calcd for $C_{21}H_{24}NO_5$, 370.1648).

Compound 2. Yellowish amorphous powder; $[\alpha]_D^{25}$ −55.6 (*c* 0.90, MeOH); IR (ATR) ν_{max}: 2940, 1753, 1623, 1511, 1462, 1365, 1266, 1180, 1064, 873, 798 cm^{-1}; UV (MeOH) λ_{max} (log ε): 209 (4.93), 276 (3.93) nm; ECD (MeOH) λ_{max} ($\Delta\varepsilon$) 206 (−14.21), 240 (−63.97), 286 (−2.69) nm; ^{1}H-NMR ($CDCl_3$, 400 MHz), and ^{13}C-NMR ($CDCl_3$, 100 MHz) data: see Tables 1 and 2; ESI-TOF-MS *m*/*z* 412.1747 $[M + H]^+$ (calcd for $C_{23}H_{26}NO_6$, 412.1754).

Compound 3. Yellowish amorphous powder; $[\alpha]_D^{25}$ −165.7 (*c* 0.69, MeOH); IR (ATR) ν_{max}: 2936, 1758, 1619, 1512, 1459, 1367, 1265, 1187, 1065, 911, 798 cm^{-1}; UV (MeOH) λ_{max} (log ε): 204 (5.99), 278 (4.96) nm; ECD (MeOH) λ_{max} ($\Delta\varepsilon$) 206 (−8.98), 240 (−49.83), 286 (−8.12) nm; ^{1}H-NMR ($CDCl_3$, 400 MHz), and ^{13}C-NMR ($CDCl_3$, 100 MHz) data: see Tables 1 and 2; ESI-TOF-MS *m*/*z* 412.1748 $[M + H]^+$ (calcd for $C_{23}H_{26}NO_6$, 412.1754).

Compound 4. Pale yellowish amorphous powder; $[\alpha]_D^{25}$ −74.3 (*c* 0.16, MeOH); IR (ATR) ν_{max}: 3314, 2923, 1611, 1512, 1456, 1259, 1067, 870, 798 cm^{-1}; UV (MeOH) λ_{max} (log ε): 202 (3.64), 284 (2.70) nm; ECD (MeOH) λ_{max} ($\Delta\varepsilon$) 211 (−11.55), 234 (−41.99), 290 (−4.32) nm; ^{1}H-NMR (CD_3OD, 400 MHz), and ^{13}C-NMR (CD_3OD, 100 MHz) data: see Tables 1 and 2; ESI-TOF-MS *m*/*z* 490.2056 $[M + H]^+$ (calcd for $C_{25}H_{32}NO_9$, 490.2071).

Compound 5. Brownish amorphous powder; $[\alpha]_D^{26}$ −26.6 (*c* 0.30, MeOH); IR (ATR) ν_{max}: 3383, 2900, 2837, 1603, 1575, 1498, 1414, 1236, 1031, 982 cm^{-1}; UV (MeOH) λ_{max} (log ε): 218 (3.79), 283 (3.54) nm; ECD (MeOH) λ_{max} ($\Delta\varepsilon$) 216 (+13.95), 238 (−36.48), 269 (+33.45), 297 (+2.79), 307 (−20.33) nm; ^{1}H-NMR (CD_3OD, 400 MHz), and ^{13}C-NMR (CD_3OD, 100 MHz) data: see Tables 3 and 4; ESI-TOF-MS *m*/*z* 312.1224 $[M + Na]^+$ (calcd for $C_{18}H_{18}NNaO_4$, 312.1230).

Compound 6. Pale yellowish amorphous solid; $[\alpha]_D^{25}$ + 5.8 (*c* 0.51, H_2O); IR (ATR) ν_{max}: 3311, 2905, 1593, 1427, 1321, 1255, 1067 cm^{-1}; UV (MeOH) λ_{max} (log ε): 210 (3.85), 272 (3.52) nm; ECD (H_2O) λ_{max} ($\Delta\varepsilon$) 211 (−34.47), 232 (+69.01), 270 (−9.83), 297 (−0.16), 315 (+7.29) nm; ^{1}H-NMR (CD_3OD, 400 MHz), and ^{13}C-NMR (CD_3OD, 100 MHz) data: see Tables 3 and 4; ESI-TOF-MS *m*/*z* 430.1856 $[M + H]^+$ (calcd for $C_{23}H_{28}NO_7$, 430.1860).

Compound 7. Brownish amorphous powder; IR (ATR) ν_{max}: 3276, 2923, 1638, 1574, 1458, 1234, 1030, 967 cm^{-1}; UV (MeOH) λ_{max} (log ε): 206 (3.80), 247 (3.72), 275 (3.67) nm; ^{1}H-NMR (CD_3OD, 400 MHz), and ^{13}C-NMR (CD_3OD, 100 MHz) data: see Tables 3 and 4; ESI-TOF-MS *m*/*z* 344.0523 $[M + Na]^+$ (calcd for $C_{18}H_{11}NNaO_5$, 344.0529).

Compound 8. Brownish amorphous powder; IR (ATR) ν_{max}: 2938, 1651, 1583, 1460, 1250, 1162, 1038, 968 cm^{-1}; UV (MeOH) λ_{max} (log ε): 219 (3.55), 244 (3.68), 307 (3.25), 319 (3.32) nm; ^{1}H-NMR ($CDCl_3$, 400 MHz), and ^{13}C-NMR ($CDCl_3$, 100 MHz) data: see Tables 3 and 4; ESI-TOF-MS *m*/*z* 388.0772 $[M + Na]^+$ (calcd for $C_{20}H_{15}NNaO_6$, 388.0791).

Compound 9. Pale brownish amorphous powder; $[\alpha]_D^{26}$ −361.6 (*c* 1.32, $CHCl_3$); IR (ATR) ν_{max}: 2937, 1761, 1636, 1417, 1367, 1244, 1193, 1085 cm^{-1}; ECD (MeOH) λ_{max} ($\Delta\varepsilon$) 218 (+31.45), 235 (−39.64), 270 (+11.81), 297 (+2.89), 307 (−37.83) nm; ^{1}H-NMR (CD_3OD, 400 MHz), and ^{13}C-NMR (CD_3OD, 100 MHz) data: see Tables 3 and 4; ESI-TOF-MS *m*/*z* 374.1363 $[M + Na]^+$ (calcd for $C_{21}H_{21}NNaO_4$, 374.1362).

Compound 10. Pale yellowish amorphous solid; IR (ATR) ν_{max}: 2928, 1751, 1595, 1541, 1449, 1277, 1036, 987 cm^{-1}; ^{1}H-NMR ($CDCl_3$, 400 MHz), and ^{13}C-NMR ($CDCl_3$, 100 MHz) data: see Table 5; ESI-TOF-MS *m*/*z* 382.1258 $[M + H]^+$ (calcd for $C_{22}H_{24}NO_5$, 382.1648).

Compound 11. Pale yellowish amorphous solid; $[\alpha]_D^{25}$ −195.0 (*c* 0.60, MeOH); IR (ATR) ν_{max}: 3380, 2921, 1606, 1495, 1448, 1267, 1123, 1063, 874, 773 cm^{-1}; ^{1}H-NMR (DMSO-d_6, 400 MHz), and ^{13}C-NMR (DMSO-d_6, 100 MHz) data: see Tables 1 and 2; ESI-TOF-MS *m*/*z* 328.1542 $[M + H]^+$ (calcd for $C_{19}H_{22}NO_4$, 328.1543).

Enzymatic hydrolysis of compounds 4 and 6

Compound **4** (0.5 mg) was dissolved in water (0.5 mL) and the mixture was incubated with Sigma β-glucosidase (from almonds, 1.0 mg) at 37–38 °C for 5 h.[51] The reaction mixture was extracted with ethyl acetate and the solvent was removed *in vacuo*. TLC comparison with discretamine (**13**)[22] isolated from *S. pierrei* in the present work revealed the identity of the aglycone with **13**. The aqueous layer was concentrated and analyzed by TLC comparison with authentic D-glucose using $CHCl_3$: MeOH : H_2O (3 : 1.5 : 0.2).

Compound **6** was similarly hydrolyzed under the same condition and the aglycone and the sugar were similarly analyzed.

Evaluation of AChE and BuChE inhibitory activities

AChE (from *Electrophorus electricus*), BuChE (from equine serum), galanthamine (as hydrobromide salt), 5,5′-dithiobis(2-nitrobenzoic acid) (DTNB), bovine serum albumin (BSA), acetylthiocholine iodide (ATCI) and *S*-butyrylthiocholine iodide (BTCI) were purchased from Sigma-Aldrich (St. Louis, Misouri, USA). AChE and BuChE inhibitory activities were conducted by using Ellman's method with slight modification.[66] Briefly, the enzyme solutions were prepared at 0.2 unit per mL in 10 mM phosphate buffer solution (PBS, pH 8.0). The assay medium consisted of 20 μL of the enzyme, 140 μL of 10 mM PBS and 20 μL of tested compounds were mixed in a 96-well plate and shaken for 10 min. The reaction was initiated by the addition of 20 μL of a mixture of 5 mM DTNB, 0.1% BSA, and substrate (ATCI or BTCI). The hydrolysis of ASCI was monitored by the yellow 5-thio-2-nitrobenzoate anion formation as a result of the reaction with DTNB and thiocholines, catalyzed by enzymes at a wavelength of 405 nm and the absorbance was measured by using a microplate reader (Sunrise, Switzerland) after 5 min of incubation at room temperature. The percentage of inhibition was calculated by comparing the rate of enzymatic hydrolysis of ASCI for the sample to that of the blank (80% MeOH in buffer). Similarly, BuChE inhibition was performed as described for AChE. All samples were run in triplicate in 96-well microplates and galanthamine was used as a positive control.

$$\text{Enzyme inhibitory activity assay (\%)} = [(\text{absorbance of control} - \text{absorbance of sample})/\ \text{absorbance of control}] \times 100.$$

The IC_{50} values were determined graphically from inhibition curves (inhibitor concentration *vs.* percent of inhibition) and each concentration was performed in triplicate.

Molecular docking calculations

The three-dimensional (3D) structures of human AChE in complex with galanthamine and human BuChE in complex with tacrine were obtained from Protein Data Bank with PDB IDs: 4EY6 [67] (resolution: 2.40 Å) and 4BDS[65] (resolution: 2.10 Å), respectively. The water molecules were removed and all missing hydrogen atoms were added to this protein using AutoDockTools (ADT).[68] The potent alkaloids were structurally sketched using ACDLab[69] and optimized at the Hartree-Fock level with a 6-31G basis set using the Gaussian 03 program[70] and then converted to mol^2 format using GaussView[71] for docking study. The Autodock 4.2 program[68] was used to examine the binding affinity of the optimized alkaloid structures towards the binding site of AChE and BuChE proteins. Non-polar hydrogens and lone pairs were merged and partial atomic charges were assigned using the Gasteiger method.[72] The protein molecule was set rigid throughout the docking, while the ligand compounds were allowed to be flexible by the rotation parameter. The cubical grid box of 80 × 80 × 80 points with a spacing of 0.375 Å was positioned at the active site of the cholinesterase proteins. Galanthamine and tacrine were re-docked into the binding pockets of AChE and BuChE, respectively, to serve as controls. Autogrid4 was used to attain a rigid grid maps. Then, autodock4 was used with Lamarckian genetic algorithms and by default of the protocol to gain the 200 independent docking runs. After the run, the docked conformation with the lowest binding energy in the most populated cluster of each compound was selected for detailed analysis and further studies. Visualization of the docking results was

performed using Acceryls Discovery Studio 2.5 (Acceryls, Inc., San Diego, CA, USA).

Conclusions

In summary, eight new alkaloids (**1–8**), three new naturally occurring alkaloids (**9–11**), together with thirty-four known alkaloids (**12–45**), have been isolated from *Stephania pierrei* tubers. Most of the isolated compounds were evaluated for acetylcholinesterase (AChE) and butyrylcholinesterase (BuChE) inhibitory activities. Compound **42** exhibited the most potent AChE inhibitory effect, followed by compound **38**, which were respectively slightly more active than and comparable to galanthamine. Moreover, compound **23** exhibited the highest BuChE inhibitory activity, which was 1.3-fold more active than galanthamine, followed by compounds **22**, **38** and **39** which also showed high inhibitory activity. Molecular docking studies are well in agreement with these experimental results. The alkaloids **42** and **23** may respectively be regarded as lead compounds for anti-AChE and anti-BuChE drug development.

Author contributions

Waraluck Chaichompoo: methodology, investigation, data curation, formal analysis, visualization, and writing – original draft. Pornchai Rojsitthisak: conceptualization, resources, supervision, funding acquisition, project administration, and writing – review & editing. Wachirachai Pabuprapap: investigation, data curation, formal analysis, visualization, and writing – review & editing. Yuttana Siriwattanasathien: investigation, validation, data curation, and formal analysis. Pathumwadee Yotmanee: investigation, data curation, formal analysis, software, and writing – review & editing. Woraphot Haritakun: investigation, and data curation. Apichart Suksamrarn: conceptualization, resources, supervision, funding acquisition, project administration, and writing – review & editing.

Conflicts of interest

The authors declare no conflict of interest.

Acknowledgements

The authors express gratitude to the Thailand Science Research and Innovation (TSRI) Fund (CU_FRB640001_01_33_3), the Ratchadaphiseksomphot Endowment Fund for the Natural Products for Ageing and Chronic Diseases, Chulalongkorn University (GRU 6404733002-1) (P. R.) and The Thailand Research Fund (DBG6180030) (A. S. and P. R.). This research is supported by Ratchadapisek Somphot Fund for Postdoctoral Fellowship, Chulalongkorn University (W. C.). Support from the Center of Excellence for Innovation in Chemistry, Ministry of Higher Education, Science, Research and Innovation is gratefully acknowledged.

Notes and references

1 Alzheimer's Association, *Alzheimers. Dement.*, 2020, **16**, 391–460.
2 T. McLaughlin, H. Feldman, H. Fillit, M. Sano, F. Schmitt, P. Aisen, C. Leibman, L. Mucha, J. M. Ryan, S. D. Sullivan, D. E. Spackman, P. J. Neumann, J. Cohen and Y. Stern, *Alzheimers. Dement.*, 2010, **6**, 482–493.
3 Alzheimer's Disease International, *World Alzheimer Report 2019: Attitudes to dementia*, Alzheimer's Disease International, London, 2019.
4 Y. Ju, H. Chakravarty and K. Y. Tam, *ACS Chem. Neurosci.*, 2020, **11**, 3346–3357.
5 H. A. Hassan, A. E. Allam, D. H. Abu-Baih, M. F. A. Mohamed, U. R. Abdelmohsen, K. Shimizu, S. Y. Desoukey, A. M. Hayallah, M. A. Elrehany, K. M. Mohamedi and M. S. Kamel, *RSC Adv.*, 2020, **10**, 36920–36929.
6 M. M. Mesulam, A. Guillozet, P. Shaw, A. Levey, E. G. Duysen and O. Lockridge, *Neuroscience*, 2002, **110**, 627–639.
7 J. Gabriel, M. R. Almeida, M. H. Ribeiro, J. Duraes, M. Tabuas-Pereira, A. C. Pinheiro, R. Pascoal, I. Santana and I. Baldeiras, *Neurosci. Lett.*, 2017, **641**, 101–106.
8 D. G. Wilkinson, P. T. Francis, E. Schwam and J. Payne-Parrish, *Drugs Aging*, 2004, **21**, 453–478.
9 F. Zemek, L. Drtinova, E. Nepovimova, V. Sepsova, J. Korabecny, J. Klimes and K. Kuca, *Expert Opin. Drug Saf.*, 2014, **13**, 759–774.
10 P. Patil, A. Thakur, A. Sharma and S. J. S. Flora, *Drug Dev. Res.*, 2020, **81**, 165–183.
11 D. M. Pereira, F. Ferreres, J. M. A. Oliveira, L. Gaspar, J. Faria, P. Valentão, M. Sottomayor and P. B. Andrade, *Phytomedicine*, 2010, **17**, 646–652.
12 E. L. Konrath, C. S. Passos, L. C. Klein-Júnior and A. T. Henriques, *J. Pharm. Pharmacol.*, 2013, **65**, 1701–1725.
13 D. K. Semwal, R. Badoni, R. Semwal, S. K. Kothiyal, G. J. P. Singh and U. Rawat, *J. Ethnopharmacol.*, 2010, **132**, 369–383.
14 T. Smitinand, *Thai Plant Names, Rev. Edit. Office of the Forest Herbarium, Department of Natural Park, Wildlife and Plant Conservation*, Bangkok, 2014.
15 C. Dary, S. Hul, S. Kim and F. Jabbour, *Edinb. J. Bot.*, 2015, **72**, 423–428.
16 K. Likhitwitayawuid, C. K. Angerhofer, H. Chai, J. M. Pezzuto and G. A. Cordell, *J. Nat. Prod.*, 1993, **56**, 1468–1478.
17 J. Maliwong, P. Sahakitpichan, N. Chimnoi, S. Ruchirawat and T. Kanchanapoom, *Phytochem. Lett.*, 2021, **43**, 140–144.
18 M. Tomita and M. Kozuka, *Yakugaku Zasshi*, 1965, **85**, 77–82.
19 H. Wang, X. Cheng, S. Kong, Z. Yang, H. Wang, Q. Huang, J. Li, C. Chen and Y. Ma, *Molecules*, 2016, **21**, 1555.
20 W. Xiao, X. Zhuang, G. Shen, Y. Zhong, M. Yuan and H. Li, *J. Sep. Sci.*, 2014, **37**, 696–703.
21 K. Ingkaninan, P. Phengpa, S. Yuenyongsawad and N. Khorana, *J. Pharm. Pharmacol.*, 2006, **58**, 695–700.
22 J. R. G. S. Almeida, J. T. Lima, H. R. Oliveira, M. R. Oliveira, P. R. M. Meira, A. S. S. C. Lucio, J. M. Barbosa Filho and L. J. Quintans Junior, *Nat. Prod. Res.*, 2011, **25**, 1908–1915.

23 S. Nantapap, C. Loetchutinat, P. Meepowpan, N. Nuntasaen and W. Pompimon, *Am. J. Appl. Sci.*, 2010, **7**, 1057–1065.
24 S. Singh, T. D. Singh, V. P. Singh and V. B. Pandey, *Pharm. Biol.*, 2010, **48**, 158–160.
25 Y. D. Min, M. C. Yang, K. H. Lee, K. R. Kim, S. U. Choi and K. R. Lee, *Arch. Pharmacal Res.*, 2006, **29**, 757–761.
26 S. Tong and J. Yan, *J. Liq. Chromatogr. Relat. Technol.*, 2005, **28**, 2979–2989.
27 T. M. Hung, M. K. Na, N. T. Dat, T. M. Ngoc, U. J. Youn, H. J. Kim, B. S. Min, J. P. Lee and K. H. Bae, *J. Ethnopharmacol.*, 2008, **119**, 74–80.
28 J. I. Kunitomo, Y. Okamoto, E. Yuge and Y. Nagai, *Yakugaku Zasshi*, 1969, **89**, 1691–1695.
29 J. T. Blanchfield, D. P. A. Sands, C. H. L. Kennard, K. A. Byriel and W. Kitching, *Phytochemistry*, 2003, **63**, 711–720.
30 F. Roblot, R. Hocquemiller and A. Cave, *J. Nat. Prod.*, 1983, **46**, 862–873.
31 W. G. Ma, Y. Fukushi, S. Tahara and T. Osawa, *Fitoterapia*, 2000, **71**, 527–534.
32 C. Y. Chen, F. R. Chang and Y. C. Wu, *J. Chin. Chem. Soc.*, 1997, **44**, 313–319.
33 B. Tantisewie and K. Pharadai, *J. Nat. Prod.*, 1982, **45**, 355–357.
34 C. Dary, S. S. Bun, G. Herbett, F. Mabrouki, H. Bun, S. Kim, F. Jabbour, S. Hul, B. Baghdikian and E. Ollivier, *Nat. Prod. Res.*, 2017, **31**, 802–809.
35 E. M. K. Wijeratne, Y. Hatanaka, T. Kikuchi, Y. Tezuka and A. A. L. Gunatilaka, *Phytochemistry*, 1996, **42**, 1703–1706.
36 B. N. Zhou, R. K. Johnson, M. R. Mattern, X. Wang, S. M. Hecht, H. T. Beck, A. Ortiz and D. G. I. Kingston, *J. Nat. Prod.*, 2000, **63**, 217–221.
37 M. Leboeuf and A. Cave, *Phytochemistry*, 1972, **11**, 2833–2840.
38 P. H. Guinaudeau, M. Leboeuf, M. Debray, A. Cave and R. R. Paris, *Planta Med.*, 1975, **27**, 304–318.
39 J. I. Kunitomo, M. Oshikata and M. Akasu, *Yakugaku Zasshi*, 1981, **101**, 951–955.
40 X. Wang, J. Qi, P. Zhao, C. Liu, M. Yang, H. Wang, Y. Y. Hu, Z. Liao and X. Xia, *Chem. Nat. Compd.*, 2020, **56**, 572–575.
41 M. P. Cava, Y. Watanabe, K. Bessho and M. J. Mitchell, *Tetrahedron Lett.*, 1968, **20**, 2437–2442.
42 D. H. Le, K. Nishimura and T. Tanahashi, *Nat. Prod. Commun.*, 2016, **11**, 949–952.
43 E. V. Costa, M. F. C. Sampaio, M. J. Salvador, A. Nepele and A. Barison, *Quim. Nova*, 2015, **38**, 769–776.
44 F. Bracher, W. J. Eisenreich, J. Muhlbacher, M. Dreyer and G. Bringmann, *J. Org. Chem.*, 2004, **69**, 8602–8608.
45 H. Corrodi and E. Hardegger, *Helv. Chim. Acta*, 1956, **39**, 889–897.
46 R. Hocquemiller, C. Debitus, F. Roblot and A. Cave, *J. Nat. Prod.*, 1984, **47**, 353–362.
47 S. G. Pyne and B. Dikic, *J. Org. Chem.*, 1990, **55**, 1932–1936.
48 B. Ringdahl, R. P. K. Chan, J. C. Craig and R. H. F. Manske, *J. Nat. Prod.*, 1981, **44**, 75–79.
49 S. M. Hu, S. X. Xu, X. S. Yao, C. C. Cui, Y. Tezuka and T. Kikuchi, *Chem. Pharm. Bull.*, 1993, **41**, 1866–1868.
50 P. Suebsakwong, W. Chulrik, W. Chunglok, J. X. Li, Z. J. Yao and A. Suksamrarn, *RSC Adv.*, 2020, **10**, 10461–10470.
51 L. T. Byrne, J. M. Sasse, B. W. Skelton, A. Suksamrarn and A. H. White, *Aust. J. Chem.*, 1987, **40**, 785–794.
52 H. X. Ge, J. Zhang, C. Kai, J. H. Liu and B. Y. Yu, *Appl. Microbiol. Biotechnol.*, 2012, **93**, 2357–2364.
53 L. M. Jackman, J. C. Trewella, J. L. Moniot, M. Shamma, R. L. Stephens, E. Wenkert, M. Leboeuf and A. Cavé, *J. Nat. Prod.*, 1979, **42**, 437–449.
54 M. Shamma, *The isoquinoline alkaloids*, Academic Press, New York, 1972.
55 M. Shamma and J. L. Moniot, *Experientia*, 1975, **32**, 282–283.
56 Y. W. Ge, S. Zhu, M. Y. Shang, X. Y. Zang, X. Wang, Y. J. Bai, L. Li, K. Komatsu and S. Q. Cai, *Phytochemistry*, 2013, **86**, 201–207.
57 B. Ringdahl, R. P. K. Chan, J. C. Craig, M. P. Cava and M. Shamma, *J. Nat. Prod.*, 1981, **44**, 80–85.
58 F. N. Samita, L. P. Sandjo, I. O. Ndiege, A. Hassanali and W. Lwande, *Beilstein J. Org. Chem.*, 2013, **9**, 447–452.
59 W. Silprakob, N. Sukhamsri, C. Kuhakarn, S. Hongthong, S. Jariyawat, K. Suksen, R. Akkarawongsapat, J. Limthongkul, N. Nantasaen and V. Reutrakul, *Nat. Prod. Commun.*, 2018, **13**, 1471–1474.
60 T. M. Hung, N. H. Dang, J. C. Kim, H. S. Jang, S. W. Ryoo, J. H. Lee, J. S. Choi, K. H. Bae and B. S. Min, *Planta Med.*, 2010, **76**, 1762–1764.
61 J. W. Dong, L. Cai, Y. S. Fang, H. Xiao, Z. J. Li and Z. T. Ding, *Fitoterapia*, 2015, **104**, 102–107.
62 X. P. Kong, H. Q. Ren, E. Y. L. Liu, K. W. Leung, S. C. Guo, R. Duan, T. T. X. Dong and K. W. K. Tsim, *Molecules*, 2020, **25**, 5914.
63 L. Cai, J. W. Dong, L. X. Zhao, H. Zhou, Y. Xing, Y. Li, Z. J. Li, W. H. Duan, X. J. Li and Z. T. Ding, *Process Biochem.*, 2016, **51**, 933–940.
64 J. Cheung, M. J. Rudolph, F. Burshteyn, M. S. Cassidy, E. N. Gary, J. Love, M. C. Franklin and J. J. Height, *J. Med. Chem.*, 2012, **55**, 10282–10286.
65 F. Nachon, E. Carletti, C. Ronco, M. Trovaslet, Y. Nicolet, L. Jean and P. Y. Renard, *Biochem. J.*, 2013, **453**, 393–399.
66 G. L. Ellman, K. D. Courtney, V. Andres and R. M. Featherstone, *Biochem. Pharmacol.*, 1961, **7**, 88–95.
67 J. Cheung, M. J. Rudolph, F. Burshteyn, M. S. Cassidy, E. N. Gary, J. Love, M. C. Franklin and J. J. Height, *J. Med. Chem.*, 2012, **55**, 10282–10286.
68 G. M. Morris, R. Huey, W. Lindstrom, M. F. Sanner, R. K. Belew, D. S. Goodsell and A. J. Olson, *J. Comput. Chem.*, 2009, **16**, 2785–2791.
69 *Acdlabs.com. ACD/ChemSketch for Academic and Personal Use :ACD/Labs.com, 2015*. [online] available at: http://www.acdlabs.com/resources/freeware/chemsketch/ [accessed 2 May 2015].
70 M. J. Frisch, *et al.*, *Gaussian 03, Revision C.02*, Gaussian, Inc., Wallingford CT, 2004.
71 R. Dennington, T. Keith and J. Millam. *GaussView*, Semichem Inc., Shawnee Mission KS., 2009.
72 J. Gasteiger and M. Marsili, *Tetrahedron*, 1980, **36**, 3219–3228.